Neutrino dynamics below the electroweak crossover

JCAP07(2016)015

(http://iopscience.iop.org/1475-7516/2016/07/015)

Journal of Cosmology and Astroparticle Physics
An IOP and SISSA journal

Neutrino dynamics below the electroweak crossover

J. Ghiglieri and M. Laine

AEC, Institute for Theoretical Physics, University of Bern,
Sidlerstrasse 5, CH-3012 Bern, Switzerland

E-mail: ghiglieri@itp.unibe.ch, laine@itp.unibe.ch

Received June 1, 2016
Accepted June 29, 2016
Published July 12, 2016

Abstract. We estimate the thermal masses and damping rates of active ($m < \mathrm{eV}$) and sterile ($M \sim \mathrm{GeV}$) neutrinos with thermal momenta $k \sim 3T$ at temperatures below the electroweak crossover ($5\,\mathrm{GeV} < T < 160\,\mathrm{GeV}$). These quantities fix the equilibration or "washout" rates of Standard Model lepton number densities. Sterile neutrinos interact via direct scatterings mediated by Yukawa couplings, and via their overlap with active neutrinos. Including all leading-order reactions we find that the washout rate generally exceeds the Hubble rate for $5\,\mathrm{GeV} < T < 30\,\mathrm{GeV}$. Therefore it is challenging to generate a large lepton asymmetry facilitating dark matter computations operating at $T < 5\,\mathrm{GeV}$, whereas the generation of a baryon asymmetry at $T > 130\,\mathrm{GeV}$ remains an option. Our differential rates are tabulated in a form suitable for studies of specific scenarios with given neutrino Yukawa matrices.

Keywords: leptogenesis, particle physics - cosmology connection, neutrino theory

ArXiv ePrint: 1605.07720

doi:10.1088/1475-7516/2016/07/015

JCAP07(2016)015

Contents

1 Introduction

There has been recent interest in the cosmological role that right-handed (sterile) neutrinos with masses in the GeV range could play. The dynamics of such particles may lead to a generation of a lepton asymmetry, which could explain the observed baryon asymmetry of the universe [1, 2]. The lepton asymmetry generation could continue after it cannot be converted into a baryon asymmetry any more ($T \lesssim 130\,\mathrm{GeV}$); if the resulting lepton asymmetry is several orders of magnitude larger than the baryon asymmetry, it might be resonantly converted into keV scale sterile neutrino dark matter at $T \lesssim 1\,\mathrm{GeV}$ [3]. Computations of lepton asymmetry generation have been carried out for two almost degenerate generations

JCAP07(2016)015

of sterile neutrinos [4–10], as well as for three possibly less degenerate generations [11, 12]. If the masses fall below the 0.1 GeV range (but above the 0.1 MeV range), the production is so efficient that such particles should already have been observed through the total energy density that they carry [13]. If the masses are higher but still relatively close to this lower bound, roughly $0.5 \ldots 5\,\mathrm{GeV}$ ($m_K \ldots m_B$), these particles can be searched for with the planned SHiP experiment at CERN [14]. Therefore, there is a need to refine the theoretical understanding concerning the behaviour of such particles within the ultrarelativistic plasma that filled the early universe.

Computing reliably the lepton asymmetry generated in a specific scenario is extremely challenging, because both CP violation and complicated plasma physics play a role. At the same time it is relatively straightforward to establish a constraint on whether any lepton asymmetry would be washed out after its generation (cf. e.g. refs. [15, 16] for reviews). This is in analogy with attempts to explain baryon asymmetry through an electroweak phase transition: the washout constraint $\Delta\langle\phi^\dagger\phi\rangle \gtrsim T^2/2$, where ϕ denotes a Higgs doublet and Δ a discontinuity across the transition temperature, already rules out a large class of theories, including the Standard Model which has no genuine transition. The goal of the present paper is to establish similar washout constraints for generating a large lepton asymmetry.

More precisely, we discuss a number of quantities that characterize the behaviour of GeV scale right-handed neutrinos within a plasma. One is called their "production rate": it tells how fast the particles are being produced if their initial density is much below the equilibrium value. Another is their "equilibration rate": it tells how fast the particles can adjust their number density if they are initially close to equilibrium but the temperature of the equilibrium ensemble evolves, as is the case in the early universe. Despite being conceptually different, it turns out that these quantities can be related to each other [17]. The main quantity that we consider is the lepton number "washout rate", which tells how fast any initial lepton asymmetry is being depleted in the presence of right-handed neutrinos. This rate can also be related to the rates mentioned above [18]. In the following, we frequently refer to the "production rate", with the relations to the other quantities specified in section 2.

A number of previous computations of the right-handed neutrino production rate are worth mentioning. For small masses ($M \ll \pi T$) the production rate has been computed at low temperatures $T < 5\,\mathrm{GeV}$ both for vanishing [19] and non-vanishing [20, 21] lepton asymmetries. At high temperatures $T > 160\,\mathrm{GeV}$ it has been computed in the non-relativistic $M \gg \pi T$ [22–24], relativistic $M \sim \pi T$ [25, 26], and ultrarelativistic $M \ll \pi T$ regimes [27, 28]. Computations in the ultrarelativistic regime are challenging, because they require a nested resummation of the loop expansion in order to generate a consistent weak-coupling series. An interpolation applicable for any $M/(\pi T)$ has also been suggested for $T > 160\,\mathrm{GeV}$ [29].

The status as outlined above means that there is a gap in our understanding in the range $5\,\mathrm{GeV} \lesssim T \lesssim 160\,\mathrm{GeV}$. A rough estimate was presented in appendix A of ref. [4], however this was not based on a controlled computation but just included Born level $1 \leftrightarrow 2$ processes with vacuum masses evolved through a changing Higgs expectation value. The main goal of the present paper is to fill the gap $5\,\mathrm{GeV} \lesssim T \lesssim 160\,\mathrm{GeV}$.

The paper is organized as follows. The basic observables considered are defined and the structures of the corresponding results are outlined in section 2. In section 3 we discuss right-handed neutrino production through direct $1 \leftrightarrow 2$ processes, as well as the so-called LPM resummation of the $1 + n \leftrightarrow 2 + n$ reactions that contribute at the same order in the soft regime $M, m_W \ll \pi T$. In section 4 the production through direct $2 \leftrightarrow 2$ scatterings is considered. Section 5 is devoted to "indirect" production, via an overlap with left-handed

JCAP07(2016)015

neutrinos, pointing out the importance of $2 \leftrightarrow 2$ scatterings mediated by soft gauge boson exchange at high temperatures and of $1 \to 2$ gauge boson decays at low temperatures. Numerical results are collected in section 6, and we conclude in section 7. A number of technical details and remarks concerning NLO effects are relegated to five appendices.

2 Summary of the setup and main results

One of the physical quantities that we are interested in is the production rate of right-handed neutrinos. The produced right-handed neutrinos have a momentum $k \equiv |\mathbf{k}|$ and a mass M. The corresponding on-shell four-momentum is denoted by $\mathcal{K} = (k_0, \mathbf{k})$, where $k_0 = \sqrt{k^2 + M^2}$. In light of the scenario relevant for SHiP [14], we consider here small masses, $M \leq 16\,\mathrm{GeV}$, and high temperatures, $T \geq 5\,\mathrm{GeV}$. Then the right-handed neutrinos can be considered to be "ultrarelativistic", with momenta $k \sim \pi T$ and masses $M \ll \pi T$.

Let h_{Ia} be a neutrino Yukawa coupling, $a \in \{1,2,3\}$ a left-handed lepton generation index, and $I \in \{1,2,3\}$ a right-handed neutrino generation index, defined in a basis in which the Majorana mass matrix is real and diagonal:

$$\mathcal{L} = \mathcal{L}_{\rm SM} + \frac{1}{2}\sum_I \bar{N}_I\big(i\gamma^\mu\partial_\mu - M_I\big)N_I - \sum_{I,a}\Big(\bar{N}_I\, h_{Ia}\tilde{\phi}^\dagger a_{\rm L}\,\ell_a + \bar{\ell}_a\, a_{\rm R}\,\tilde{\phi}\, h^*_{Ia} N_I\Big)\,. \tag{2.1}$$

Here $\tilde{\phi} = i\sigma_2\phi^*$ is a Higgs doublet; $a_{\rm L}, a_{\rm R}$ are chiral projectors; and $\ell_a = (\nu\, e)^T_a$ is a left-handed lepton doublet. For notational simplicity we normally suppress the generation index in a Majorana mass, i.e. $M_I \to M$.

We consider time scales large enough that all Standard Model (SM) degrees of freedom are in thermal equilibrium. However quantities whose interactions involve the h_{Ia}, notably right-handed neutrino phase space distributions ($\equiv f_{I\mathbf{k}}$) and Standard Model lepton densities ($\equiv n_a$), can be out of equilibrium. The task is to determine the equilibration rates of these observables. We note that n_a can be carried both by neutral and by charged leptons.

For $T \geq 5\,\mathrm{GeV}$, all Standard Model leptons can be considered degenerate and massless ($\pi T \gg m_\tau \approx 1.8\,\mathrm{GeV}$). Then the dynamical information concerning the rates of interest is contained in the 2-point function of the operator to which the right-handed neutrinos couple [17]. For computational convenience we first define the corresponding imaginary-time correlator,

$$\Pi_{\rm E}(K) \equiv {\rm Tr}\left\{ i\not{K}\int_0^{1/T}{\rm d}\tau\int_{\mathbf{x}} e^{iK\cdot X}\left\langle(\tilde{\phi}^\dagger a_{\rm L}\,\ell)(X)\,(\bar{\ell}\,a_{\rm R}\,\tilde{\phi})(0)\right\rangle_T\right\}\,, \tag{2.2}$$

where $K \equiv (k_n, \mathbf{k})$ and k_n is a fermionic Matsubara frequency. Moreover, $X \equiv (\tau, \mathbf{x})$ denotes a Euclidean space-time coordinate and $\langle\ldots\rangle_T$ an equilibrium expectation value. The retarded correlator $\Pi_{\rm R}$ can be expressed as an analytic continuation of $\Pi_{\rm E}$ as

$$\Pi_{\rm R}(\mathcal{K}) = \Pi_{\rm E}(K)|_{k_n\to -i[k_0+i0^+]}\,, \tag{2.3}$$

and the rate observables are proportional to the spectral function $\rho \equiv {\rm Im}\,\Pi_{\rm R}$.

We choose a normalization for the phase distribution function $f_{I\mathbf{k}}$ such that the total number density of right-handed neutrinos, summed over the two spin states, reads

$$n_I = \int_{\mathbf{k}} 2 f_{I\mathbf{k}}\,, \quad \int_{\mathbf{k}} \equiv \int\frac{{\rm d}^3\mathbf{k}}{(2\pi)^3}\,. \tag{2.4}$$

JCAP07(2016)015

Denoting $k_0 \equiv E_I$ for the mass M_I, it can be shown that [17]

$$\dot{f}_{I\mathbf{k}} = \gamma_{I\mathbf{k}} \left(n_{\rm F}(E_I) - f_{I\mathbf{k}} \right) + \mathcal{O}\big[\big(n_{\rm F} - f_{I\mathbf{k}} \big)^2, n_a^2 \big] \,, \tag{2.5}$$

where the right-hand side was expanded to leading order in small lepton densities, $\dot{f}$ refers to a covariant time derivative in an expanding phase space background, and $n_{\rm F}$ denotes the Fermi distribution (similarly, $n_{\rm B}$ denotes a Bose distribution).[1] The coefficient $\gamma_{I\mathbf{k}}$ can be called the (spin-averaged) "*equilibration rate*", and is given by

$$\gamma_{I\mathbf{k}} = \sum_a \frac{|h_{Ia}|^2 \, \mathrm{Im}\, \Pi_{\rm R}(\mathcal{K})}{E_I} + \mathcal{O}(h^4) \,. \tag{2.6}$$

This relation applies to all orders in Standard Model couplings.

Normally, when referring to the right-handed neutrino *"production rate"*, it is assumed that their number density is small, $f_{I\mathbf{k}} \ll n_{\rm F}$. For this case eqs. (2.4) and (2.5) imply that

$$\dot{n}_I = \sum_a \int_{\mathbf{k}} \frac{2 n_{\rm F}(E_I) |h_{Ia}|^2 \, \mathrm{Im}\, \Pi_{\rm R}(\mathcal{K})}{E_I} + \mathcal{O}(h^4, n_I) \,. \tag{2.7}$$

The same processes by which right-handed neutrinos equilibrate or are produced also violate lepton densities carried by Standard Model particles. Because lepton numbers are violated, their equilibrium values vanish. Close to equilibrium, the lepton densities evolve as

$$\dot{n}_a = -\gamma_{ab} \, n_b + \mathcal{O}\big[n_a (n_{\rm F} - f_{I\mathbf{k}}), n_a^3 \big] \,, \tag{2.8}$$

where the matrix of decay coefficients, or *"washout rates"*, can be written as [18]

$$\gamma_{ab} = -\sum_I \int_{\mathbf{k}} \frac{2 n_{\rm F}'(E_I) |h_{Ia}|^2 \, \mathrm{Im}\, \Pi_{\rm R}(\mathcal{K})}{E_I} \, \Xi^{-1}_{ab} + \mathcal{O}(h^4) \,. \tag{2.9}$$

Here $\Xi_{ab} = \partial n_a / \partial \mu_b |_{\mu_b = 0} \sim T^2$ is a susceptibility matrix related to lepton densities. It was determined up to next-to-next-to-leading order (NNLO) in Standard Model couplings at $T \gtrsim 160\,\mathrm{GeV}$ in ref. [30], and leading-order results valid for $T \lesssim 160\,\mathrm{GeV}$ are given in appendix A. We note that Ξ is non-diagonal, because the plasma as a whole is charge neutral, so that changes in the number densities of different lepton flavours are correlated.

As is clear from eqs. (2.6), (2.7) and (2.9), the dynamical information that we need is contained in the function $\mathrm{Im}\, \Pi_{\rm R}$, obtained from eq. (2.3). We now turn to its determination.

In order to carry out a theoretically consistent computation, power-counting rules need to be established for the various scales appearing in the problem. We denote by h_t the renormalized top Yukawa coupling; by $N_{\rm c} \equiv 3$ the number of colours; by g_1, g_2 the hypercharge and weak gauge couplings; and by λ the Higgs self-coupling. The notation g^2 refers generically to the couplings $g_1^2, g_2^2, h_t^2, \lambda$ which are taken to be parametrically of the same order of magnitude, and "small" in the sense that $g^2 \ll \pi^2$.

Suppose that we are at a temperature $T < 160\,\mathrm{GeV}$ so that, in gauge-fixed perturbation theory, the neutral component of the Higgs field has an expectation value. The expectation value is denoted by v; at $T = 0$, $v \simeq 246\,\mathrm{GeV}$. We mainly consider a regime in which

[1] The generalization of eq. (2.5) to finite lepton densities can be found in eq. (2.21) of ref. [20]. Similarly, the generalization of eq. (2.8) to off-equilibrium right-handed neutrinos can be found in eq. (2.24) of ref. [20].

JCAP07(2016)015

(a) (b)

Figure 1. (a) Examples of $1+n \leftrightarrow 2+n$ processes for the direct generation of right-handed neutrinos from a Yukawa interaction. (b) Examples of $1+n \leftrightarrow 2+n$ processes for the generation of left-handed neutrinos which subsequently oscillate into right-handed ones. Arrowed, dashed, and wiggly lines correspond to Standard Model fermions, scalars, and gauge bosons, respectively, whereas right-handed neutrinos are denoted by a double line. The closed blob includes a Higgs expectation value.

(a) (b)

Figure 2. (a) Examples of $2 \to 2$ processes for the direct generation of right-handed neutrinos from a Yukawa interaction. (b) Examples of $2 \to 2$ processes for the generation of left-handed neutrinos which subsequently oscillate into right-handed ones. The notation is as in figure 1. The complete set for case (a) is shown in figure 1 of ref. [29] and for case (b) in figure 7 below.

$v \lesssim T$, even though the case $m_W \gtrsim \pi T$, i.e. $v \gtrsim \pi T/g$, is considered as well. For $v \lesssim T$ vacuum masses $\sim gv$ are of the same order as thermal masses $\sim gT$ but much smaller than typical momenta $k \sim \pi T$. In other words, all particles can be considered to be ultrarelativistic. Based on various numerical tests, this regime is numerically applicable in a rather broad temperature range,

$$30\,\mathrm{GeV} \lesssim T \lesssim 160\,\mathrm{GeV}\,. \tag{2.10}$$

At lower temperatures, Higgs and gauge bosons become non-relativistic and need to be decoupled from the computation (the top quark becomes non-relativistic already at a somewhat higher temperature).

In the regime of eq. (2.10), there are two types of contributions to $\mathrm{Im}\,\Pi_{\mathrm{R}}$. First, the Higgs field $\tilde{\phi}$ in eq. (2.2) can represent a propagating mode (Goldstone or Higgs). This leads to the same processes as have previously been considered in the symmetric phase [27, 28]; examples of $1+n \leftrightarrow 2+n$ processes are shown in figure 1(a) and of $2 \leftrightarrow 2$ processes in figure 2(a). Second, the Higgs field could be replaced by its expectation value, $\tilde{\phi} \simeq (v\,0)^T/\sqrt{2}$. Then we are left to consider processes experienced by an active (left-handed) neutrino. Examples of amplitudes are illustrated in figures 1(b) and 2(b). We refer to first type as a "direct" contribution and to the second as an "indirect" one.

When amplitudes such as those in figures 1 and 2 are squared, there are no interference terms between the direct and indirect sets, provided that we adopt a class of gauges (such as the R_ξ gauge) in which scalar and gauge fields do not transform to each other. Then the rate can be written as

$$\mathrm{Im}\,\Pi_{\mathrm{R}} \;=\; \mathrm{Im}\,\Pi_{\mathrm{R}}|_{\mathrm{direct}} \;+\; \mathrm{Im}\,\Pi_{\mathrm{R}}|_{\mathrm{indirect}}\;, \tag{2.11}$$

where the "direct" processes are like in sets (a) of figures 1 and 2. Like in the symmetric phase [27, 28], the direct term has the parametric magnitude $\mathrm{Im}\,\Pi_{\mathrm{R}}|_{\mathrm{direct}} \sim g^2T^2$ (recalling

JCAP07(2016)015

that $|h_{Ia}|^2$ has been factored out). In contrast the indirect term has a more complicated structure (cf. section 5.1),

$$\mathrm{Im}\,\Pi_{\mathrm{R}}|_{\mathrm{indirect}} \;=\; \frac{v^2}{2}\,\frac{M^2 k_0\Gamma}{(M^2-m_\ell^2)^2+k_0^2\Gamma^2}\;, \tag{2.12}$$

where m_ℓ is the active neutrino thermal mass in the ultrarelativistic regime (cf. eq. (3.2)),[2] and Γ is its thermal width (cf. eq. (5.7)). The term in eq. (2.12) is proportional to v^2 because it originates from processes induced by electroweak symmetry breaking, and to M^2 because in the massless limit helicity and fermion number conservation would forbid transitions between left and right-handed states.

We note in passing that, in an alternative language, the combination $|h_{Ia}|^2v^2M^2/\{2[(M^2-m_\ell^2)^2+k_0^2\Gamma^2]\}$ originating from eq. (2.12) can be interpreted as a medium-modified mixing angle squared. This weights the part of the interaction rate $k_0\Gamma$ of the weak eigenstates that is transmitted to the sterile mass eigenstates. The interaction rate $k_0\Gamma$ also appears in the denominator of the effective mixing angle, thereby contributing towards the "unitarity" of the conversion process. Nevertheless, because M^2 and m_ℓ^2 can cancel against each other, the medium-modified mixing angle can be much larger than the vacuum one.

Now, an essential ingredient in our analysis is the determination of the active neutrino interaction rate Γ. We find that, because of strong infrared enhancement, $\Gamma\sim g^2T/\pi$ in the regime of eq. (2.10), cf. eq. (5.33). For $k_0\sim k\sim\pi T$ we thus get

$$\mathrm{Im}\,\Pi_{\mathrm{R}}|_{\mathrm{indirect}} \;\sim\; \frac{v^2}{2}\,\frac{M^2 g^2T^2}{(M^2-g^2T^2)^2+g^4T^4}\;. \tag{2.13}$$

This implies that for $M\sim gT$ we get $\mathrm{Im}\,\Pi_{\mathrm{R}}|_{\mathrm{indirect}}\sim v^2\sim T^2$, i.e. the indirect production dominates over the direct one. The direct production dominates only if we go to the symmetric phase ($v\lesssim gT/\pi$ if $M\sim gT$, or $v\lesssim T$ if $M\sim g^2T/\pi$).

In order to consolidate these findings, we proceed to discuss $\mathrm{Im}\,\Pi_{\mathrm{R}}|_{\mathrm{direct}}$ and $\mathrm{Im}\,\Pi_{\mathrm{R}}|_{\mathrm{indirect}}$. We start from the former, considering the $1+n\leftrightarrow 2+n$ and $2\to 2$ contributions in turn, and return to the indirect processes in section 5.

3 Direct $1+n\leftrightarrow 2+n$ scatterings

3.1 LPM resummation in the symmetric phase

An essential ingredient in the physics of the processes illustrated in figure 1(a) is the proper inclusion of the so-called Landau-Pomeranchuk-Migdal (LPM) resummation. Because of phase space suppression, the rate of the $1\leftrightarrow 2$ process (after factoring out $|h_{Ia}|^2$) is $\sim m^2\sim g^2T^2$, where m denotes vacuum or thermal masses. On the other hand, adding gauge scatterings to the $1\leftrightarrow 2$ result leads to no further suppression, because the exchanged gauge boson is soft, with a virtuality $\sim g^2T^2$. Therefore all the gauge scatterings need to be resummed in order to obtain the correct leading-order result.

Starting with the symmetric phase, the basic equations for the LPM resummation can be summarized as follows [27]. We define

$$\hat{H} \;\equiv\; -\frac{M^2}{2k_0}+\frac{m_\ell^2-\nabla_\perp^2}{2\omega_1}+\frac{m_\phi^2-\nabla_\perp^2}{2\omega_2}-i\,\Gamma(y)\quad y\equiv|\mathbf{y}_\perp|\;, \tag{3.1}$$

[2] When we exit the ultrarelativistic regime, $-m_\ell^2$ is replaced by a more complicated function, cf. section 5.2.

JCAP07(2016)015

where $\nabla_\perp$ is a two-dimensional gradient operating in directions orthogonal to $\mathbf{k}$, and the thermal masses of hard particles (with $k \gg m$) read

$$m_\ell^2 = \frac{(g_1^2+3g_2^2)T^2}{16}\,, \quad m_\phi^2 = -\frac{m_H^2}{2} + \Big(g_1^2+3g_2^2+4h_t^2+8\lambda\Big)\frac{T^2}{16}\,, \tag{3.2}$$

where $m_H \approx 125\,\mathrm{GeV}$ is the physical Higgs mass. Soft gauge scatterings are represented by a thermal width which reads

$$\Gamma(y) = \frac{T}{8\pi}\sum_{i=1}^{2} d_i\, g_i^2 \left[\ln\!\left(\frac{m_{\mathrm{E}i}y}{2}\right) + \gamma_{\mathrm{E}} + K_0\big(m_{\mathrm{E}i}y\big)\right], \tag{3.3}$$

where $d_1 \equiv 1$, $d_2 \equiv 3$, and K_0 is a modified Bessel function. The Debye masses associated with the hypercharge and SU(2) gauge fields are defined as

$$m_{\mathrm{E}1}^2 \;\equiv\; \Big(\frac{n_S}{6}+\frac{5n_G}{9}\Big)g_1^2T^2\,, \quad m_{\mathrm{E}2}^2 \;\equiv\; \Big(\frac{2}{3}+\frac{n_S}{6}+\frac{n_G}{3}\Big)g_2^2T^2\,. \tag{3.4}$$

Here $n_S \equiv 1$ is the number of Higgs doublets and $n_G \equiv 3$ the number of fermion generations. The Debye masses appear frequently in the remainder of this paper. The Hamiltonian plays a role in the inhomogeneous equations

$$(\hat{H}+i0^+)\,g(\mathbf{y}) \;=\; \delta^{(2)}(\mathbf{y})\,, \quad (\hat{H}+i0^+)\,\mathbf{f}(\mathbf{y}) \;=\; -\nabla_\perp\delta^{(2)}(\mathbf{y})\,. \tag{3.5}$$

From the solutions of these equations, the LPM-resummed contribution to $\mathrm{Im}\,\Pi_{\mathrm{R}}$ reads

$$\begin{aligned}\mathrm{Im}\,\Pi_{\mathrm{R}}^{\mathrm{LPM,symmetric}} \equiv{}& \frac{1}{4\pi}\int_{-\infty}^{\infty}\mathrm{d}\omega_1\int_{-\infty}^{\infty}\mathrm{d}\omega_2\;\delta(k_0-\omega_1-\omega_2)\,\big[1-n_{\mathrm{F}}(\omega_1)+n_{\mathrm{B}}(\omega_2)\big]\\ &\times\frac{k_0}{\omega_2}\lim_{\mathbf{y}\to\mathbf{0}}\left\{\frac{M^2}{k_0^2}\,\mathrm{Im}\,\big[g(\mathbf{y})\big]+\frac{1}{\omega_1^2}\,\mathrm{Im}\,\big[\nabla_\perp\cdot\mathbf{f}(\mathbf{y})\big]\right\}.\end{aligned} \tag{3.6}$$

3.2 LPM resummation in the broken phase

In the broken phase, the scalar sector splits up into Higgs and Goldstone modes. The contribution of the Goldstone modes depends strongly on the gauge choice; at tree-level, it is straightforward to verify that both the "direct" and "indirect" contributions are gauge-dependent, but their sum is gauge-independent. Once LPM resummation is incorporated, it is complicated to carry out computations in a general gauge, because this implies the presence of many different masses and correspondingly a large matrix of gauge and scalar states mixed by gauge interactions. In the following we restrict ourselves to the Feynman R_ξ gauge, which minimizes the number of different states and masses. In this gauge, the Goldstone modes correspond to the physical $W^\pm$ and Z^0 bosons, and we denote

$$m_{\phi_0}^2 \;\equiv\; 2\lambda v^2\,, \quad m_{\phi_3}^2 \;\equiv\; m_Z^2 = \frac{(g_1^2+g_2^2)v^2}{4}\,, \quad m_{\phi_1}^2 \;\equiv\; m_{\phi_2}^2 \;\equiv\; m_W^2 = \frac{g_2^2v^2}{4}\,. \tag{3.7}$$

With non-degenerate scalar masses, the Green's functions in eq. (3.5) split up into several components, $g_0,\ldots,g_3$, and similarly for $\mathbf{f}$. The LPM-resummed $1\leftrightarrow 2$ contribution can be expressed as a generalization of eq. (3.6),

$$\begin{aligned}\mathrm{Im}\,\Pi_{\mathrm{R}}^{\mathrm{LPM,broken}} \equiv{}& \frac{1}{16\pi}\int_{-\infty}^{\infty}\mathrm{d}\omega_1\int_{-\infty}^{\infty}\mathrm{d}\omega_2\;\delta(k_0-\omega_1-\omega_2)\,\big[1-n_{\mathrm{F}}(\omega_1)+n_{\mathrm{B}}(\omega_2)\big]\\ &\times\frac{k_0}{\omega_2}\lim_{\mathbf{y}\to\mathbf{0}}\sum_{\mu=0}^{3}\left\{\frac{M^2}{k_0^2}\,\mathrm{Im}\,\big[g_\mu(\mathbf{y})\big]+\frac{1}{\omega_1^2}\,\mathrm{Im}\,\big[\nabla_\perp\cdot\mathbf{f}_\mu(\mathbf{y})\big]\right\}.\end{aligned} \tag{3.8}$$

JCAP07(2016)015

Here the contributions from $\mu = 1$ and $\mu = 2$ are equal, given that the charged scalar fields ϕ_1 and ϕ_2 are degenerate. The task now is to determine the Hamiltonian $\hat{H}$ for this situation.

As a first step, we introduce notation for defining the gauge field propagators in the broken phase. Because the temporal gauge field components get thermal masses, given by eq. (3.4), the temporal and spatial gauge fields mix differently. In fact, the self-energies contain more structure than just thermal masses; in general the mixing is momentum-dependent. However, because of a sum rule derived in ref. [31] and a more general argument presented in ref. [32], the quantities of our interest (see below) can be reduced to (static) Matsubara zero mode propagators. Within the regime of validity of the Hard Thermal Loop (HTL) description [34, 35], the static self-energies are momentum independent. Therefore mixing can be described by constant angles, separate for spatial and temporal gauge fields.

The standard weak mixing angle can be defined as

$$\sin(2\theta) \;\equiv\; \frac{2g_1 g_2}{g_1^2 + g_2^2}\,. \tag{3.9}$$

Denoting $s \equiv \sin\theta$, $c \equiv \cos\theta$ and adopting a convention according to which a covariant derivative acting on the Higgs doublet reads $D_\mu\phi \;\equiv\; \left(\partial_\mu + \frac{ig_1}{2}B_\mu - ig_2 T^a A^a_\mu\right)\phi$, where $\mathrm{Tr}\,(T^a T^b) = \delta_{ab}/2$, the spatial gauge field components can be diagonalized as

$$A^3_i = cZ_i - sQ_i\,, \quad B_i = sZ_i + cQ_i\,, \quad i \in \{1,2,3\}\,, \tag{3.10}$$

where Q_μ is the massless photon field and B_μ is the hypercharge field. The mixing angle of the static temporal components is denoted by $\tilde{\theta}$, and is given by

$$\sin(2\tilde{\theta}) \;\equiv\; \frac{\sin(2\theta)m_Z^2}{\sqrt{\sin^2(2\theta)m_Z^4 + [\cos(2\theta)m_Z^2 + m_{\mathrm{E2}}^2 - m_{\mathrm{E1}}^2]^2}}\,. \tag{3.11}$$

Denoting $\tilde{s} \equiv \sin\tilde{\theta}$, $\tilde{c} \equiv \cos\tilde{\theta}$, the zero components are diagonalized by

$$A^3_0 = \tilde{c}\tilde{Z}_0 - \tilde{s}\tilde{Q}_0\,, \quad B_0 = \tilde{s}\tilde{Z}_0 + \tilde{c}\tilde{Q}_0\,. \tag{3.12}$$

All diagonal fields have non-zero masses because of the thermal corrections in eq. (3.4):

$$m^2_{\tilde{W}} \equiv m_W^2 + m_{\mathrm{E2}}^2\,, \quad m^2_{\tilde{Z}} \;\equiv\; m_+^2\,, \quad m^2_{\tilde{Q}} \;\equiv\; m_-^2\,, \tag{3.13}$$

$$m_\pm^2 \equiv \frac{1}{2}\Big\{m_Z^2 + m_{\mathrm{E1}}^2 + m_{\mathrm{E2}}^2 \pm \sqrt{\sin^2(2\theta)m_Z^4 + [\cos(2\theta)m_Z^2 + m_{\mathrm{E2}}^2 - m_{\mathrm{E1}}^2]^2}\Big\}\,. \tag{3.14}$$

The gauge field combinations to which neutral and charged left-handed leptons couple, respectively, are $Z_0 \equiv cA^3_0 + sB_0$, $Z'_0 \equiv -cA^3_0 + sB_0$. In the diagonal basis the corresponding propagators become

$$\langle Z_0 Z_0\rangle \;=\; \cos^2(\theta-\tilde{\theta})\,\langle\tilde{Z}_0\tilde{Z}_0\rangle + \sin^2(\theta-\tilde{\theta})\,\langle\tilde{Q}_0\tilde{Q}_0\rangle\,, \tag{3.15}$$

$$\langle Z'_0 Z'_0\rangle \;=\; \cos^2(\theta+\tilde{\theta})\,\langle\tilde{Z}_0\tilde{Z}_0\rangle + \sin^2(\theta+\tilde{\theta})\,\langle\tilde{Q}_0\tilde{Q}_0\rangle\,. \tag{3.16}$$

These structures appear frequently below.

Now, we return to the thermal width, denoted by Γ in eq. (3.1). Choosing $\mathbf{k}$ to point in the x_3-direction, nearly light-like particles couple to the gauge field components A_0 and A_3. In a thermal plasma, the soft scatterings mediated by these components are not identical,

JCAP07(2016)015

and the final result originates from the difference of the two contributions. Because of a sum rule [31, 32], the result can most simply be expressed in terms of the static Matsubara zero-mode sector ($q_n = 0$) related to these gauge potentials. In the static limit the propagators of temporal components can be expressed as in eqs. (3.15) and (3.16). We define the widths related to $W^\pm$, Z, and Z' exchanges as

$$\Gamma_{W}(y) \equiv \frac{g_2^2 T}{4}\int_{\mathbf{q}_\perp} e^{i\mathbf{q}_\perp\cdot\mathbf{y}}\left[\frac{1}{q_\perp^2+m_{W}^2}-\frac{1}{q_\perp^2+m_{\widetilde{W}}^2}\right], \tag{3.17}$$

$$\Gamma_{Z}(y) \equiv \frac{(g_1^2+g_2^2)T}{4}\int_{\mathbf{q}_\perp} e^{i\mathbf{q}_\perp\cdot\mathbf{y}}\left[\frac{1}{q_\perp^2+m_{Z}^2}-\frac{\cos^2(\theta-\tilde{\theta})}{q_\perp^2+m_{\tilde{Z}}^2}-\frac{\sin^2(\theta-\tilde{\theta})}{q_\perp^2+m_{\tilde{Q}}^2}\right], \tag{3.18}$$

$$\Gamma_{Z'}(y) \equiv \frac{(g_1^2+g_2^2)T}{4}\int_{\mathbf{q}_\perp} e^{i\mathbf{q}_\perp\cdot\mathbf{y}}\left[\frac{\cos^2(2\theta)}{q_\perp^2+m_{Z}^2}+\frac{\sin^2(2\theta)}{q_\perp^2}-\frac{\cos^2(\theta+\tilde{\theta})}{q_\perp^2+m_{\tilde{Z}}^2}-\frac{\sin^2(\theta+\tilde{\theta})}{q_\perp^2+m_{\tilde{Q}}^2}\right], \tag{3.19}$$

where $\int_{\mathbf{q}_\perp} \equiv \int \frac{\mathrm{d}^{2-2\epsilon}\mathbf{q}_\perp}{(2\pi)^{2-2\epsilon}}$ and $q_\perp \equiv |\mathbf{q}_\perp|$. Dimensional regularization has been used for defining the value of an infrared divergent integral in eq. (3.19), related to soft photon exchange, even though this divergence soon drops out (cf. the discussion below eq. (3.21)). The full width matrix, in the space of neutral and charged scalars and leptons that participate in the production of right-handed neutrinos, ordered as $\nu\phi_0$, $\nu\phi_3$, $e\phi_1$, $e\phi_2$, reads

$$\Gamma_{4\times4} = \begin{pmatrix} 2\Gamma_{W}(0)+\Gamma_{Z}(0) & -\Gamma_{Z}(y) & -\Gamma_{W}(y) & -\Gamma_{W}(y) \\ -\Gamma_{Z}(y) & 2\Gamma_{W}(0)+\Gamma_{Z}(0) & -\Gamma_{W}(y) & -\Gamma_{W}(y) \\ -\Gamma_{W}(y) & -\Gamma_{W}(y) & 2\Gamma_{W}(0)+\Gamma_{Z'}(0) & -\Gamma_{Z'}(y) \\ -\Gamma_{W}(y) & -\Gamma_{W}(y) & -\Gamma_{Z'}(y) & 2\Gamma_{W}(0)+\Gamma_{Z'}(0) \end{pmatrix}. \tag{3.20}$$

The arguments 0 and y correspond to self-energy and exchange contributions, respectively. The combination $2\Gamma_{W}(0)+\Gamma_{Z}(0)$ corresponds to the active neutrino width or interaction rate, re-derived in some more detail in section 5.5 (cf. eq. (5.33)).

Given that the pairs $e\phi_1$ and $e\phi_2$ are degenerate, we can choose one of them as a representative. Then, the matrix in eq. (3.20) can be reduced into a 3×3 form,

$$\Gamma_{3\times3} = \begin{pmatrix} 2\Gamma_{W}(0)+\Gamma_{Z}(0) & -\Gamma_{Z}(y) & -2\Gamma_{W}(y) \\ -\Gamma_{Z}(y) & 2\Gamma_{W}(0)+\Gamma_{Z}(0) & -2\Gamma_{W}(y) \\ -\Gamma_{W}(y) & -\Gamma_{W}(y) & 2\Gamma_{W}(0)+\Gamma_{Z'}(0)-\Gamma_{Z'}(y) \end{pmatrix}. \tag{3.21}$$

A nice consequence of this reduction is that infrared divergences related to photon exchange cancel in the combination $\Gamma_{Z'}(0)-\Gamma_{Z'}(y)$. To be explicit,

$$\Gamma_{W}(y) = \frac{g_2^2 T}{8\pi}\Big[K_0(m_W y)-K_0(m_{\widetilde{W}}y)\Big], \tag{3.22}$$

$$\Gamma_{W}(0) = \frac{g_2^2 T}{8\pi}\ln\frac{m_{\widetilde{W}}}{m_W}, \tag{3.23}$$

$$\Gamma_{Z}(y) = \frac{(g_1^2+g_2^2)T}{8\pi}\Big[K_0(m_Z y)-\cos^2(\theta-\tilde{\theta})K_0(m_{\tilde{Z}}y)-\sin^2(\theta-\tilde{\theta})K_0(m_{\tilde{Q}}y)\Big], \tag{3.24}$$

$$\Gamma_{Z}(0) = \frac{(g_1^2+g_2^2)T}{8\pi}\Big[\cos^2(\theta-\tilde{\theta})\ln\frac{m_{\tilde{Z}}}{m_Z}+\sin^2(\theta-\tilde{\theta})\ln\frac{m_{\tilde{Q}}}{m_Z}\Big], \tag{3.25}$$

JCAP07(2016)015

whereas the difference in the bottom-right component takes the form

$$\begin{aligned}\Gamma_{Z'}(0) - \Gamma_{Z'}(y) \;=\; \frac{(g_1^2+g_2^2)T}{8\pi}\Bigg\{&\cos^2(\theta+\tilde\theta)\left[K_0(m_{\tilde Z}y) + \ln\frac{m_{\tilde Z}y}{2} + \gamma_{\rm E}\right] \\ &+ \sin^2(\theta+\tilde\theta)\left[K_0(m_{\tilde Q}y) + \ln\frac{m_{\tilde Q}y}{2} + \gamma_{\rm E}\right] \\ &- \cos^2(2\theta)\left[K_0(m_Z y) + \ln\frac{m_Z y}{2} + \gamma_{\rm E}\right]\Bigg\}\,. \end{aligned} \tag{3.26}$$

With the width determined, let us generalize the Hamiltonian of eq. (3.1) to contain a diagonal mass matrix,

$$m_\phi^2 \;\to\; \mathrm{diag}(m_{\phi_0}^2, m_{\phi_3}^2, m_{\phi_1}^2)\,. \tag{3.27}$$

The Green's functions g and $\mathbf{f}$ are generalized to 3-component vectors. With the 3×3 width $\Gamma_{3\times 3}$, we can then solve eq. (3.5), and insert the result into eq. (3.8).

As a crosscheck, we note that in the symmetric phase, the parameters appearing in eqs. (3.22)–(3.26) behave as $m_W \to 0, m_Z \to 0$, $\tilde\theta \to 0$, $m_{\overline W} \to m_{\rm E2}$, $m_{\tilde Z} \to m_{\rm E2}$, $m_{\tilde Q} \to m_{\rm E1}$, and $\Gamma_{Z'} \to \Gamma_Z$. Moreover all the pairs $\nu\phi_0$, $\nu\phi_3$, $e\phi_1$ and $e\phi_2$ become degenerate, so we can reduce the 3×3 matrix into a single function,

$$\Gamma_{1\times 1} \;=\; \lim_{m_W, m_Z\to 0}\Big\{2\big[\Gamma_W(0) - \Gamma_W(y)\big] + \Gamma_Z(0) - \Gamma_Z(y)\Big\}\,. \tag{3.28}$$

Noting that $\lim_{m\to 0}[K_0(my) + \ln\frac{my}{2} + \gamma_{\rm E}] = 0$, this agrees with eq. (3.3).

For a numerical solution, we make use of the general approach of ref. [33], adapted to the problem at hand in ref. [29]. The idea is to express the solutions of the inhomogeneous equations, eq. (3.5), in terms of the solutions of the homogeneous equation which are regular at origin. Choosing the normalizations of the regular solutions as

$$u^r_{\ell,\mu}(\rho) \;=\; \rho^{1/2+|\ell|}\left[1 + \mathcal{O}(\rho^2)\right]\,, \quad \mu \in \{0,1,2,3\}\,, \tag{3.29}$$

where $\rho \equiv m_{\rm E2}\, y$ and ℓ is an angular quantum number, we find

$$\begin{aligned}\mathrm{Im}\,\Pi_{\rm R}^{\rm LPM,broken} \;=\; &\frac{1}{4\pi^2}\int_{-\infty}^{\infty}\mathrm{d}\omega\,\big[1 - n_{\rm F}(\omega) + n_{\rm B}(k_0-\omega)\big] \\ &\times\sum_{\mu=0}^{3}\int_0^\infty \mathrm{d}\rho\left[\frac{\omega M^2}{4k_0^2}\,\mathrm{Im}\left\{\frac{1}{[u^r_{0,\mu}(\rho)]^2}\right\} + \frac{m_{\rm E2}^2}{\omega}\,\mathrm{Im}\left\{\frac{1}{[u^r_{1,\mu}(\rho)]^2}\right\}\right]\,. \end{aligned} \tag{3.30}$$

Here, as before, $k_0 \equiv \sqrt{k^2+M^2}$ and the kinematic range $M \ll k$ is assumed. The numerical solution is straightforward, with a result as illustrated in figure 3 (the solid lines at high temperatures).[3]

[3]Numerics can be sped up by realizing that the off-diagonal elements in eq. (3.21) fall off exponentially for $y \gg m_W^{-1}, m_{\overline W}^{-1}, m_Z^{-1}, m_{\tilde Z}^{-1}, m_{\tilde Q}^{-1}$. For large enough ρ one can then switch to three separate solvers for the three independent $u^r_{\ell,\mu}(\rho)$. This is particularly advantageous for $T \lesssim 60\,\mathrm{GeV}$, where a large tree-level term is present, which requires integration to large values of ρ to reach the required accuracy.

JCAP07(2016)015

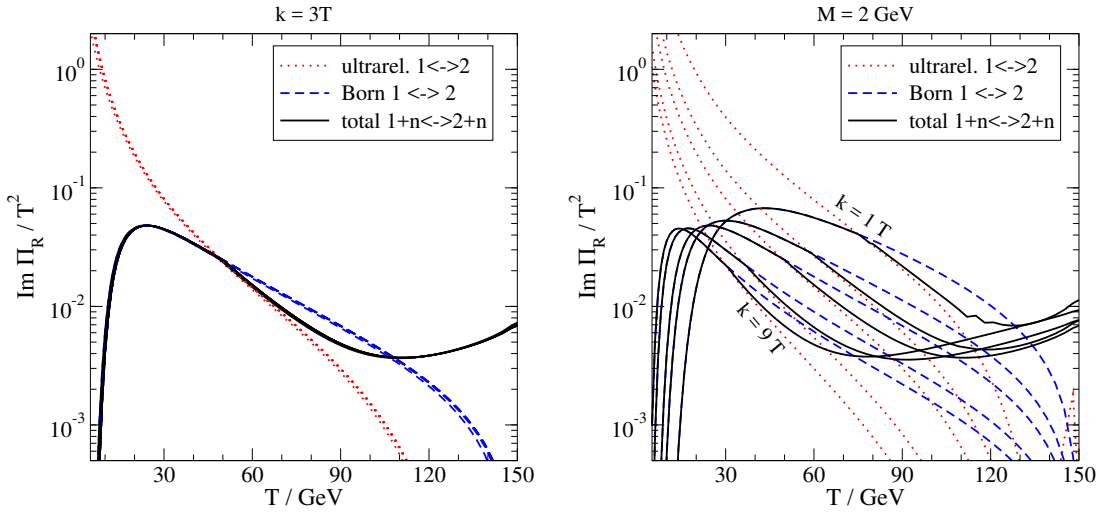

Figure 3. The direct $1+n \leftrightarrow 2+n$ contribution to $\mathrm{Im}\,\Pi_{\mathrm{R}}/T^2$. Shown are the Born result with collinear kinematics and thermal masses ("ultrarel. $1 \leftrightarrow 2$"), the naive Born result ("Born $1 \leftrightarrow 2$", cf. eq. (3.31)), as well as the LPM result going over to the Born result at low T ("total $1+n \leftrightarrow 2+n$"). The naive Born rate includes no (chirally invariant) thermal lepton mass [37] and therefore becomes too large in the regime where m_ℓ is substantial. Left: fixed $k = 3T$ and masses $M/\mathrm{GeV} \in \{0.5, 1, 2, 4, 8, 16\}$. Right: fixed $M = 2\,\mathrm{GeV}$ and momenta $k/T \in \{1, 2, 3, 6, 9\}$.

3.3 Limit of low temperatures

Once we go deep in the broken phase, the masses m_{ϕ_μ} defined in eq. (3.7) eventually become large, $m_{\phi_\mu}^2/k_0 \gg g^2T/(8\pi)$. Then $\Gamma_{3\times3}$ represents a small correction compared with the mass terms in eq. (3.5), and can be omitted. However, the collinear approximation $m_{\phi_\mu}^2/k_0 \ll k_0$ that is employed in the formalism of the LPM resummation also breaks down in the same regime. In this situation the rate is given just by the $1 \leftrightarrow 2$ processes, without any resummation nor kinematic approximation. The hard thermal lepton mass m_ℓ can also be omitted at low temperatures. Then the result can be given in a closed form,

$$\mathrm{Im}\,\Pi_{\mathrm{R}}^{\mathrm{Born}} = \sum_{\mu=0}^{3} \mathcal{F}(m_{\phi_\mu})\,, \tag{3.31}$$

$$\mathcal{F}(m) \equiv \frac{(M^2-m^2)T}{32\pi k} \ln\left\{ \frac{\sinh\left[\frac{k_+ + m^2/(4k_+)}{2T}\right] \cosh\left[\frac{k_+ - m^2/(4k_-)}{2T}\right]}{\sinh\left[\frac{k_- + m^2/(4k_-)}{2T}\right] \cosh\left[\frac{k_- - m^2/(4k_+)}{2T}\right]} \right\}\,, \tag{3.32}$$

where we have defined

$$k_\pm \equiv \frac{k_0 \pm k}{2}\,. \tag{3.33}$$

Actually, $M \ll m_{\phi_\mu}$ so that eq. (3.32) could be simplified by setting $M \to 0$ (cf. eq. (5.15)). In our numerical solution we switch from the LPM resummed result of eq. (3.30) to the Born term of eq. (3.31) when the two results cross at low T, cf. figure 3.

JCAP07(2016)015

4 Direct $2 \leftrightarrow 2$ scatterings

4.1 Ultrarelativistic regime

We now move on to discuss direct $2 \to 2$ scatterings, illustrated in figure 2(a). As long as we are in the ultrarelativistic regime, $m_W \ll \pi T$, or $v \lesssim T$, the masses of the "real" particles participating in these processes play no practical role, because all the scatterers have hard momenta $\sim \pi T$. Therefore, to leading order, the computation can be directly taken over from the symmetric phase [28]. The techniques we employ here are similar to those in ref. [28], except for the treatment of soft momentum transfer, where a mild modification is adopted. In this section we describe the computation of the direct $2 \to 2$ scatterings in some detail, in order to prepare the ground for the generalization to the indirect case in sections 5.4 and 5.5.

In the $2 \to 2$ scatterings of figure 2(a), the particles mediating t-channel exchange can have soft momenta. However, an explicit computation shows that only the lepton exchange is so infrared (IR) sensitive that the thermal lepton mass plays a role. The computation is organized by first determining the contribution from hard momentum transfer by using massless propagators, and subsequently treating the case of soft momentum transfer more carefully.

In naive massless perturbation theory, the hard part can be written as

$$\begin{aligned} & 2n_{\rm F}(k_0)\,\mathrm{Im}\,\Pi_{\rm R}\big|^{\rm hard}_{\rm direct,\,2\to2} \\ & = \int \mathrm{d}\Omega_{2\to2} \Big\{ n_{\rm B}(p_1)\, n_{\rm B}(p_2)\, \big[1 - n_{\rm F}(k_1)\big]\, \frac{1}{2}\, |\mathcal{M}_{\rm a}|^2 \\ & \qquad + n_{\rm B}(p_1)\, n_{\rm F}(p_2)\, \big[1 + n_{\rm B}(k_1)\big]\, \sum |\mathcal{M}_{\rm b}|^2 \\ & \qquad + n_{\rm F}(p_1)\, n_{\rm F}(p_2)\, \big[1 - n_{\rm F}(k_1)\big]\, \sum |\mathcal{M}_{\rm c}|^2 \Big\} \,. \end{aligned} \tag{4.1}$$

Here $\mathrm{d}\Omega_{n\to m}$ denotes the usual phase space integration measure with 4-momentum conservation, $\mathrm{d}\Omega_{n\to m} \equiv \Pi_{i=1}^{n} \frac{\mathrm{d}^3\mathbf{p}_i}{2p_i(2\pi)^3} \Pi_{j=1}^{m-1} \frac{\mathrm{d}^3\mathbf{k}_j}{2k_j(2\pi)^3}\, (2\pi)^4\, \delta^{(4)}(\sum_{i=1}^{n} \mathcal{P}_i - \sum_{j=1}^{m} \mathcal{K}_j)$. The three-momenta of incoming particles are denoted by $\mathbf{p}_i$, with $p_i \equiv |\mathbf{p}_i|$; those of outgoing particles are $\mathbf{k}_i$, with $\mathbf{k}_m \equiv \mathbf{k}$ the right-handed neutrino momentum. The matrix elements squared read

$$|\mathcal{M}_{\rm a}|^2 \equiv \big(g_1^2 + 3g_2^2\big) \left(\frac{u}{t} + \frac{t}{u}\right) , \tag{4.2}$$

$$\sum |\mathcal{M}_{\rm b}|^2 \equiv -\big(g_1^2 + 3g_2^2\big) \left(\frac{u}{s} + \frac{s}{u}\right) , \tag{4.3}$$

$$\sum |\mathcal{M}_{\rm c}|^2 \equiv 6h_t^2 N_{\rm c} \,. \tag{4.4}$$

Here $s \equiv (\mathcal{P}_1 + \mathcal{P}_2)^2$, $t \equiv (\mathcal{K}_2 - \mathcal{P}_2)^2$, and $u \equiv (\mathcal{K}_2 - \mathcal{P}_1)^2$.

The phase space integrals can be reduced into 2-dimensional integrals as explained in ref. [28]. Different parametrizations are introduced for s and t-channel exchange (the u-channel can be transformed into the t-channel by the exchange $p_1 \leftrightarrow p_2$). Defining the notation

$$\ln_{\rm f}^{-} \equiv \ln\Big(1 + e^{-|q_-|/T}\Big) \,, \qquad \ln_{\rm f}^{+} \equiv \ln\Big(1 + e^{-q_+/T}\Big) \,, \tag{4.5}$$

$$\ln_{\rm b}^{-} \equiv \ln\Big(1 - e^{-|q_-|/T}\Big) \,, \qquad \ln_{\rm b}^{+} \equiv \ln\Big(1 - e^{-q_+/T}\Big) \,, \tag{4.6}$$

$$\mathrm{li}_{i\rm f}^{-} \equiv \mathrm{Li}_i\Big(-e^{-|q_-|/T}\Big) \,, \qquad \mathrm{li}_{i\rm f}^{+} \equiv \mathrm{Li}_i\Big(-e^{-q_+/T}\Big) \,, \tag{4.7}$$

$$\mathrm{li}_{i\rm b}^{-} \equiv \mathrm{Li}_i\Big(e^{-|q_-|/T}\Big) \,, \qquad \mathrm{li}_{i\rm b}^{+} \equiv \mathrm{Li}_i\Big(e^{-q_+/T}\Big) \,, \tag{4.8}$$

JCAP07(2016)015

where

$$q_\pm \;\equiv\; \frac{q_0 \pm q}{2}\,, \tag{4.9}$$

the result reads

$$\begin{aligned}
&(4\pi)^3 k_0\,\mathrm{Im}\,\Pi_{\mathrm{R}}\big|^{\mathrm{hard}}_{\mathrm{direct},\,2\to2} \\
&\quad= \int_{k_0}^{\infty}\mathrm{d}q_+\int_0^{k_0}\mathrm{d}q_-\,\Big\{\big[n_{\mathrm{B}}(q_0)+n_{\mathrm{F}}(q_0-k_0)\big]\,\Phi_{s1} + \big[n_{\mathrm{F}}(q_0)+n_{\mathrm{B}}(q_0-k_0)\big]\,\Phi_{s2}\Big\} \\
&\qquad+\int_0^{k_0}\mathrm{d}q_+\int_{-\infty}^{0}\mathrm{d}q_-\,\Big\{\big[1-n_{\mathrm{F}}(q_0)+n_{\mathrm{B}}(k_0-q_0)\big]\,\Phi_{t2}\Big\}\,.
\end{aligned} \tag{4.10}$$

Here Φ_{s1} refers to bosonic and Φ_{s2} to fermionic s-channel exchange, and Φ_{t2} to fermionic t-channel exchange; the notation Φ_{t1} is reserved for bosonic t-channel exchange that does not appear here (or rather, appears as a diagram but does not lead to non-trivial kinematic dependence). The functions appearing in eq. (4.10) are

$$\Phi_{s1} \;=\; 6h_t^2 N_{\mathrm{c}}\left[q + 2T(\ln_{\mathrm{f}}^{+} - \ln_{\mathrm{f}}^{-})\right]\,, \tag{4.11}$$

$$\begin{aligned}
\Phi_{s2} \;=\; (g_1^2+3g_2^2)\,\Big\{&\frac{q}{2}+\frac{T}{q}\big[(k_0-q_-)(\ln_{\mathrm{f}}^{+}-\ln_{\mathrm{b}}^{-})+(k_0-q_+)(\ln_{\mathrm{f}}^{-}-\ln_{\mathrm{b}}^{+})\big] \\
&+\frac{T^2}{q^2}(2k_0-q_0)\big(\mathrm{li}_{2\mathrm{b}}^{+}+\mathrm{li}_{2\mathrm{f}}^{-}-\mathrm{li}_{2\mathrm{f}}^{+}-\mathrm{li}_{2\mathrm{b}}^{-}\big)\Big\}\,,
\end{aligned} \tag{4.12}$$

$$\begin{aligned}
\Phi_{t2} \;=\; (g_1^2+3g_2^2)\,\Big\{&\frac{T}{q}\big[(k_0-q_-)(\ln_{\mathrm{f}}^{+}-\ln_{\mathrm{b}}^{-})+(k_0-q_+)(\ln_{\mathrm{f}}^{-}-\ln_{\mathrm{b}}^{+})\big] \\
&+\frac{T^2}{q^2}(2k_0-q_0)\big(\mathrm{li}_{2\mathrm{b}}^{+}+\mathrm{li}_{2\mathrm{b}}^{-}-\mathrm{li}_{2\mathrm{f}}^{+}-\mathrm{li}_{2\mathrm{f}}^{-}\big)\Big\}\,.
\end{aligned} \tag{4.13}$$

The s-channel functions Φ_{s1} and Φ_{s2} remain finite in the whole integration range, whereas the t-channel function Φ_{t2} has a divergence in the vicinity of the origin ($q, q_0 \ll k_0$):

$$\Phi_{t2} = (g_1^2+3g_2^2)\,\frac{k_0\pi^2T^2}{q^2} + \mathcal{O}\Big(\frac{1}{q}\Big)\,. \tag{4.14}$$

This divergence is not integrable and its proper treatment requires HTL resummation [34, 35], as we now explain.

Suppose that we compute $\mathrm{Im}\,\Pi_{\mathrm{R}}$ within HTL resummed perturbation theory. The HTL scalar propagator has no cut, so the HTL result has no part which would correspond to $2\to2$ scatterings with soft Higgs exchange. Therefore the Higgs can be taken to be a "hard" external particle, and its thermal mass can be omitted. This leads to

$$\mathrm{Im}\,\Pi_{\mathrm{R}}\big|^{\mathrm{HTL}}_{\mathrm{direct},\,2\to2} = \int_{-\infty}^{\infty}\mathrm{d}q_0\int_{\mathbf{q}}\frac{-2\mathcal{K}\cdot\rho_\ell(q_0,\mathbf{q})}{|\mathbf{k}-\mathbf{q}|}\,\big[1+n_{\mathrm{B}}(k_0-q_0)-n_{\mathrm{F}}(q_0)\big]\,\delta(k_0-q_0-|\mathbf{k}-\mathbf{q}|)\,, \tag{4.15}$$

where the lepton spectral function is given in eqs. (B.1)–(B.3). The lepton spectral function is parametrized by the mass given in eq. (3.2), which is purely of thermal origin, so that all left-handed leptons are degenerate. Setting $k = k_0$ and restricting to $q, q_0 \sim m_\ell \ll k_0$ where the HTL structures play a role, the constraint $\delta(k_0 - q_0 - |\mathbf{k}-\mathbf{q}|)$ in eq. (4.15) leads to

$$\mathbf{k}\cdot\mathbf{q} \;=\; k_0q_0 + \frac{q^2-q_0^2}{2} \;=\; k_0q_0 + \mathcal{O}(m_\ell^2)\,. \tag{4.16}$$

JCAP07(2016)015

Simplifying the integrand with this approximation but keeping the full integration range (the reason should become clear in a moment), we get

$$\mathrm{Im}\,\Pi_{\mathrm{R}}|^{\mathrm{HTL}}_{\mathrm{direct},\,2\to 2} \approx \frac{1}{2\pi^2}\int_{-\infty}^{k_0}\mathrm{d}q_0\int_{|q_0|}^{2k_0-q_0}\mathrm{d}q\,q\,q_0\,(\hat{\rho}_s-\hat{\rho}_0)(q_0,q)\left[n_{\mathrm{B}}(k_0)+\frac{1}{2}\right], \tag{4.17}$$

where $\hat{\rho}_s$ and $\hat{\rho}_0$ are from eqs. (B.2) and (B.3) and terms of $\mathcal{O}(m_\ell/k_0)$ have been omitted.

Now, the contribution from hard momentum transfer, eq. (4.10), is IR divergent because of the term in eq. (4.14). The reason for this divergence is that the computation leading to eq. (4.10) did *not* incorporate HTL resummation. Fortunately we can correct for this mistake a posteriori. In order to do so, we need to subtract from eq. (4.10) the "would-be" HTL contribution, which appears there in a naive perturbative form. This is obtained from eq. (4.17) by formally expanding in a weak coupling, i.e. by assuming $q, q_0 \gg m_\ell$. According to eqs. (B.2) and (B.3) this yields

$$\hat{\rho}_s-\hat{\rho}_0 \;\approx\; \frac{m_\ell^2[-\frac{q_0}{2q^2}+\frac{1}{2q_0}]\,\mathrm{Im}\,L}{q_0^2-q^2-m_\ell^2} \;\approx\; \frac{\pi m_\ell^2}{4q^3q_0}\,, \tag{4.18}$$

where terms of $\mathcal{O}(m_\ell^4)$ have been omitted. Within this approximation eq. (4.17) becomes

$$\mathrm{Im}\,\Pi_{\mathrm{R}}|^{\mathrm{HTL,\,expanded}}_{\mathrm{direct},\,2\to 2} = \frac{1}{8\pi}\int_{-\infty}^{k_0}\mathrm{d}q_0\int_{|q_0|}^{2k_0-q_0}\mathrm{d}q\,\frac{m_\ell^2}{q^2}\left[n_{\mathrm{B}}(k_0)+\frac{1}{2}\right]. \tag{4.19}$$

Taking note of eq. (3.2) and of the changes of integration variables

$$\int_{k_0}^{\infty}\mathrm{d}q_+\int_0^{k_0}\mathrm{d}q_- = \frac{1}{2}\int_{k_0}^{\infty}\mathrm{d}q_0\int_{|2k_0-q_0|}^{q_0}\mathrm{d}q\,, \quad \int_0^{k_0}\mathrm{d}q_+\int_{-\infty}^{0}\mathrm{d}q_- = \frac{1}{2}\int_{-\infty}^{k_0}\mathrm{d}q_0\int_{|q_0|}^{2k_0-q_0}\mathrm{d}q\,, \tag{4.20}$$

this agrees exactly with eq. (4.14).

The philosophy thus is to subtract eq. (4.19) from the "naive" computation of eq. (4.10). Subsequently the "soft" contribution from eq. (4.17) is added in its proper form.

Let us now compute eq. (4.17) properly. The integral contains two scales, k_0 and m_ℓ, and we evaluate it in the approximation $m_\ell \ll k_0$. The leading contribution originates from $q, q_0 \sim m_\ell$. In order to evaluate this contribution, it is advantageous to change integration variables from q, q_0 to $q_\perp, q_0$, where

$$q_\perp^2 \;\equiv\; q^2-q_\parallel^2 \;\equiv\; q^2-\frac{(\mathbf{k}\cdot\mathbf{q})^2}{k_0^2} \;\approx\; q^2-q_0^2\,, \tag{4.21}$$

where we made use of eq. (4.16). Then

$$\begin{aligned}
\mathrm{Im}\,\Pi_{\mathrm{R}}|^{\mathrm{HTL,\,soft}}_{\mathrm{direct},\,2\to 2} &\approx \frac{1}{2\pi^2}\int_{-\infty}^{k_0}\mathrm{d}q_0\int_0^{2k_0}\mathrm{d}q_\perp\,q_\perp\,q_0\,(\hat{\rho}_s-\hat{\rho}_0)\Big(q_0,\sqrt{q_0^2+q_\perp^2}\Big)\left[n_{\mathrm{B}}(k_0)+\frac{1}{2}\right] \\
&\approx \int_0^{2k_0}\frac{\mathrm{d}q_\perp\,q_\perp}{2\pi}\underbrace{\int_{-\infty}^{\infty}\frac{\mathrm{d}q_0}{\pi}\,q_0\,(\hat{\rho}_s-\hat{\rho}_0)\Big(q_0,\sqrt{q_0^2+q_\perp^2}\Big)}_{\frac{1}{2}\frac{m_\ell^2}{q_\perp^2+m_\ell^2}}\left[n_{\mathrm{B}}(k_0)+\frac{1}{2}\right] \\
&= \frac{m_\ell^2}{8\pi}\ln\left[1+\left(\frac{2k_0}{m_\ell}\right)^2\right]\left[n_{\mathrm{B}}(k_0)+\frac{1}{2}\right],
\end{aligned} \tag{4.22}$$

JCAP07(2016)015

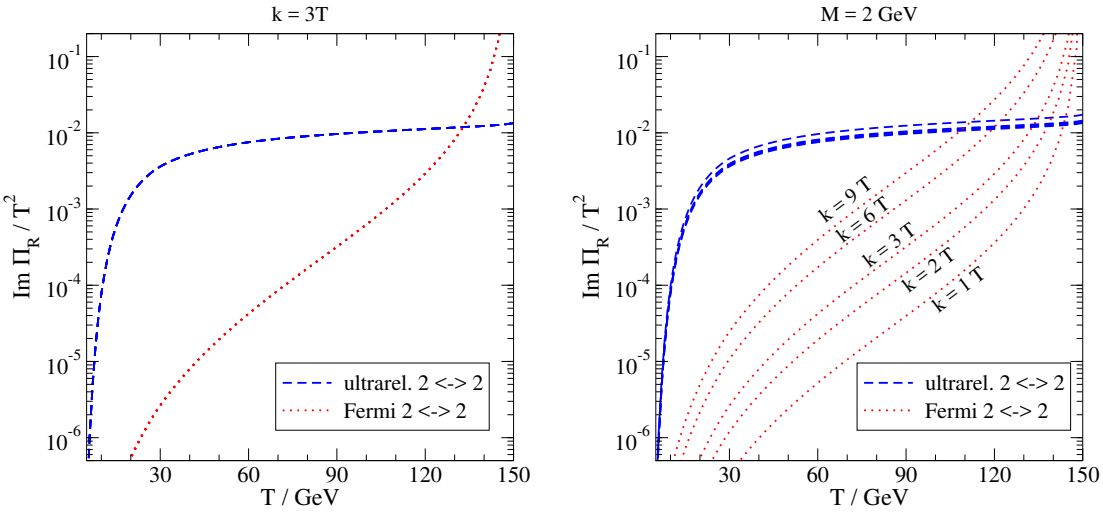

Figure 4. The direct $2 \to 2$ contribution to $\mathrm{Im}\,\Pi_\mathrm{R}/T^2$. Shown are the result from $2 \leftrightarrow 2$ scatterings treated in the ultrarelativistic approximation ("ultrarel. $1 \leftrightarrow 2$", cf. eq. (4.23)), switched off at low T as indicated at the end of section 4.2, and the leading low-T contribution ("Fermi $2 \leftrightarrow 2$", cf. eq. (4.24)). The latter is only of academic interest, because it is vanishingly small in its range of applicability, $T \lesssim 30\,\mathrm{GeV}$. Left: fixed $k = 3T$ and masses $M/\mathrm{GeV} \in \{0.5, 1, 2, 4, 8, 16\}$. Right: fixed $M = 2\,\mathrm{GeV}$.

where we employed a sum rule derived in ref. [28].[4] Putting everything together, we obtain

$$\begin{aligned}
\mathrm{Im}\,\Pi_\mathrm{R}|_{\mathrm{direct},\,2\to2} &= \mathrm{Im}\,\Pi_\mathrm{R}|^{\mathrm{hard}}_{\mathrm{direct},\,2\to2} - \mathrm{Im}\,\Pi_\mathrm{R}|^{\mathrm{HTL,\,expanded}}_{\mathrm{direct},\,2\to2} + \mathrm{Im}\,\Pi_\mathrm{R}|^{\mathrm{HTL,\,soft}}_{\mathrm{direct},\,2\to2} \\
&= \frac{1}{(4\pi)^3 k_0}\int_{k_0}^{\infty}\mathrm{d}q_+\int_0^{k_0}\mathrm{d}q_-\Big\{\big[n_\mathrm{B}(q_0)+n_\mathrm{F}(q_0-k_0)\big]\,\Phi_{s1} \\
&\qquad + \big[n_\mathrm{F}(q_0)+n_\mathrm{B}(q_0-k_0)\big]\,\Phi_{s2}\Big\} \\
&\quad + \frac{1}{(4\pi)^3 k_0}\int_0^{k_0}\mathrm{d}q_+\int_{-\infty}^{0}\mathrm{d}q_-\Big\{\big[1-n_\mathrm{F}(q_0)+n_\mathrm{B}(k_0-q_0)\big]\,\Phi_{t2} \\
&\qquad - \Big[n_\mathrm{B}(k_0)+\frac{1}{2}\Big]\,(g_1^2+3g_2^2)\,\frac{k_0\pi^2T^2}{q^2}\Big\} \\
&\quad + \frac{m_\ell^2}{4\pi}\Big[n_\mathrm{B}(k_0)+\frac{1}{2}\Big]\,\ln\!\Big(\frac{2k_0}{m_\ell}\Big) \;+\; \mathcal{O}\Big(\frac{m_\ell^4}{k_0^2}\Big)\,. \qquad (4.23)
\end{aligned}$$

This expression is IR finite and agrees with ref. [28]. Parametrically, $\mathrm{Im}\,\Pi_\mathrm{R}|_\mathrm{direct} \sim g^2T^2$. A numerical evaluation is shown in figure 4 with a dashed line ("ultrarel. $2 \leftrightarrow 2$").

4.2 Limit of low temperatures

All the $2 \leftrightarrow 2$ scattering reactions depicted in figure 2(a), leading to eqs. (4.2)–(4.4), involve a particle in the initial state whose contribution becomes exponentially suppressed when

[4] Within $\mathcal{O}(m_\ell^4/k_0^2)$ accuracy the argument of the logarithm can be simplified, cf. eq. (4.23). If however the result is evaluated numerically for small $k \lesssim gT$ where it is not leading-order correct but represents an extrapolation, it is advantageous to employ eq. (4.22) in order to avoid spurious negative expressions. We have adopted this recipe for our numerics.

JCAP07(2016)015

$m_W \gtrsim \pi T$. Therefore, the contribution of eq. (4.23) rapidly switches off once we exit the regime of eq. (2.10). Because of the resummations that were needed for obtaining eq. (4.23) it is non-trivial to obtain a general expression which has the correct high and low-temperature limits and is a smooth function in between. However, we can easily determine the low-temperature limit. The formally dominant contribution originates from Higgs mediated bottom quark scatterings. Accounting for these through a Fermi type computation and making use of the same notation as in eqs. (4.5)–(4.10), we obtain

$$\begin{aligned} \mathrm{Im}\,\Pi_{\mathrm{R}}|^{\mathrm{Fermi}}_{\mathrm{direct},\,2\to2} = {} & \frac{1}{(4\pi)^3 k_0}\int_{k_0}^{\infty}\mathrm{d}q_+\int_0^{k_0}\mathrm{d}q_-\left[n_{\mathrm{B}}(q_0)+n_{\mathrm{F}}(q_0-k_0)\right]\Phi_{s1} \\ & + \frac{1}{(4\pi)^3 k_0}\int_0^{k_0}\mathrm{d}q_+\int_{-\infty}^{0}\mathrm{d}q_-\left[1+n_{\mathrm{B}}(q_0)-n_{\mathrm{F}}(k_0-q_0)\right]\Phi_{t1}\,, \end{aligned} \tag{4.24}$$

where[5]

$$\Phi_{s1} = \sum_{\mu=0,3}\frac{h_b^2 N_{\mathrm{c}}}{m_{\phi_\mu}^4}(q_0^2-q^2)^2\left[q+2T(\ln_{\mathrm{f}}^+-\ln_{\mathrm{f}}^-)\right], \tag{4.25}$$

$$\Phi_{t1} = \sum_{\mu=0,3}\frac{h_b^2 N_{\mathrm{c}}}{m_{\phi_\mu}^4}(q_0^2-q^2)^2\left[2T(\ln_{\mathrm{f}}^--\ln_{\mathrm{f}}^+)\right]. \tag{4.26}$$

Here $h_b = g_2 m_b/(\sqrt{2}m_W) \simeq 0.03$ is the bottom quark Yukawa coupling. The result has been illustrated with a dotted line in figure 4 ("Fermi $2\leftrightarrow2$"). However, in practice this contribution is so small within its range of validity ($T \lesssim 30\,\mathrm{GeV}$) that it can be omitted.

At the same time, it is important to switch off the massless $2\leftrightarrow2$ scatterings in this regime. We have done this by multiplying $\mathrm{Im}\,\Pi_{\mathrm{R}}|_{\mathrm{direct},\,2\to2}$ of eq. (4.23) by a phenomenological factor $\kappa(m_W)$. For this we choose a "susceptibility" related to $W^\pm$ bosons (cf. eq. (A.5)), normalized to the massless limit:

$$\kappa(m_W) \equiv \frac{3}{\pi^2 T^3}\int_0^\infty \mathrm{d}p\, p^2 n_{\mathrm{B}}(E_W)[1+n_{\mathrm{B}}(E_W)]\,. \tag{4.27}$$

This has been included in the numerical "ultrarel. $2\leftrightarrow2$" results shown in figure 4. In principle it would be interesting to carry out a consistent computation for this regime, however in practice this is not necessary because, as we will see, the indirect contribution dominates the full result by many orders of magnitude at $T \lesssim 30\,\mathrm{GeV}$.

5 Indirect contribution

5.1 General structure

We now proceed to the indirect contributions, illustrated in figures 1(b) and 2(b). As a first step, let us justify the form of eq. (2.12).

According to eq. (2.2), the indirect contribution reads

$$\Pi_{\mathrm{E}}(K)|_{\mathrm{indirect}} = \frac{v^2}{2}\mathrm{Tr}\left\{i\not{K}\, a_{\mathrm{L}}\nu(-K)\bar{\nu}(0)a_{\mathrm{R}}\right\}. \tag{5.1}$$

[5] These results apply in the Feynman R_ξ gauge. In a general gauge the Goldstone mode part changes; the gauge dependence cancels against similar $2\leftrightarrow2$ indirect contributions, of the type discussed in section 5.6.

JCAP07(2016)015

It is advantageous to resum the neutrino propagator to all orders, so that the production rate remains finite even for small virtualities. The inverse neutrino propagator is of the form

$$\langle \nu(K)\bar{\nu}(0)\rangle^{-1} = i\not{K} + i\not{\Sigma}(K) \,. \tag{5.2}$$

If we make use of the property $\not{\Sigma}(-K) = -\not{\Sigma}(K)$, valid in a CP-symmetric plasma,[6] then

$$\Pi_{\rm E}(K)|_{\rm indirect} = \frac{v^2}{2}{\rm Tr}\left\{a_{\rm R} i\not{K}\,\frac{1}{-i\not{K} - i\not{\Sigma}(K)}\right\} = -v^2\,\frac{K^2 + K\cdot\Sigma}{(K+\Sigma)^2} \,. \tag{5.3}$$

After the analytic continuation in eq. (2.3), we write $\Sigma \to {\rm Re}\,\Sigma + i\,{\rm Im}\,\Sigma$. Then a few steps lead to[7]

$${\rm Im}\,\Pi_{\rm R}(\mathcal{K})|_{\rm indirect} = \frac{v^2}{2}\,\frac{M^2\, 2\mathcal{K}\cdot{\rm Im}\,\Sigma}{(M^2 + 2\mathcal{K}\cdot{\rm Re}\,\Sigma)^2 + 4(\mathcal{K}\cdot{\rm Im}\,\Sigma)^2} \,, \tag{5.4}$$

where $M^2 = \mathcal{K}^2$.

It is clear from the eq. (5.4) that an essential role in the indirect production is played by the real and imaginary parts of the (retarded) active neutrino self-energy. In the regime in which weak gauge bosons are ultrarelativistic ($m_Z \ll \pi T$), the self-energy has a Hard Thermal Loop form corresponding to eqs. (B.2) and (B.3),

$$\Sigma_{\rm HTL}(\mathcal{K}) = \left(-\frac{m_\ell^2}{2}L, \frac{m_\ell^2\,\mathbf{k}}{2k^2}(1 - k_0 L)\right) \,, \tag{5.5}$$

where m_ℓ^2 is given by eq. (3.2) and $L \equiv \frac{1}{2k}\ln\frac{k_0+k}{k_0-k}$. Then we get for the real part

$$2\mathcal{K}\cdot{\rm Re}\,\Sigma_{\rm HTL} = -m_\ell^2 \,. \tag{5.6}$$

When $m_Z \gtrsim \pi T$, the result changes; up to a normalization, $2\mathcal{K}\cdot{\rm Re}\,\Sigma$ is then referred to as a finite-temperature matter potential, whose structure is reviewed in section 5.2.

As far as the imaginary part of the active neutrino self-energy goes, we can write

$${\rm Im}\,\Sigma \;\equiv\; \left[a_i + \mathcal{O}(\mathcal{K}^2)\right]\mathcal{K} + \left[\frac{\Gamma}{2} + \mathcal{O}(\mathcal{K}^2)\right]u \,, \tag{5.7}$$

where a Lorentz-violating term proportional to the four-velocity of the heat bath $u \equiv (1, \mathbf{0})$ has been singled out. Then

$$\lim_{\mathcal{K}^2\to 0} 2\mathcal{K}\cdot{\rm Im}\,\Sigma = k_0\Gamma \,. \tag{5.8}$$

Subsequently the final expression for ${\rm Im}\,\Pi_{\rm R}$, valid for $M \ll k$, takes the form in eq. (2.12).

5.2 Finite-temperature matter potential

An important role in the indirect contribution discussed above is played by the real part of the active neutrino self-energy, $2\mathcal{K}\cdot{\rm Re}\,\Sigma$, cf. eq. (5.4), which up to a normalization is also called the finite-temperature matter potential. We review here its general form in the phase in which the Higgs mechanism is operative.

[6] We reiterature that, like in eq. (2.5), we work close to equilibrium, with vanishing lepton asymmetries.
[7] Formally we assume here that $M^2 \sim \mathcal{K}\cdot{\rm Re}\,\Sigma \sim \mathcal{K}\cdot{\rm Im}\,\Sigma \sim g^2T^2$.

JCAP07(2016)015

We work in a regime in which the right-handed neutrinos and all active leptons are ultrarelativistic, $M, m_\tau \ll \pi T$. Then $2\mathcal{K}\cdot\mathrm{Re}\,\Sigma$ is a function of two dimensionless ratios, $k/(\pi T)$ and $m_{\scriptscriptstyle G}/(\pi T)$, where $m_{\scriptscriptstyle G}$ refers to weak gauge boson masses, i.e. $G \in \{W, Z\}$. Defining

$$\lim_{\mathcal{K}^2\to 0} 2\mathcal{K}\cdot\mathrm{Re}\,\Sigma = 2g_2^2\,\mathcal{V}(m_{\scriptscriptstyle W}) + (g_1^2+g_2^2)\,\mathcal{V}(m_{\scriptscriptstyle Z})\;, \tag{5.9}$$

a straightforward computation yields

$$\begin{aligned}\mathcal{V}(m) \,=\, -\frac{1}{4\pi^2}\biggl\{ & \int_0^\infty \mathrm{d}q\, n_{\scriptscriptstyle\mathrm{F}}(q)\left[q+\frac{m^2}{8k}\ln\left|\frac{m^2-4kq}{m^2+4kq}\right|\right] \\ & + \int_m^\infty \mathrm{d}\epsilon\, n_{\scriptscriptstyle\mathrm{B}}(\epsilon)\left[\sqrt{\epsilon^2-m^2}+\frac{m^2}{8k}\ln\left|\frac{m^2-4k^2-4k\sqrt{\epsilon^2-m^2}}{m^2-4k^2+4k\sqrt{\epsilon^2-m^2}}\right|\right]\biggr\}\;,\end{aligned} \tag{5.10}$$

where $n_{\scriptscriptstyle\mathrm{F}}$ and $n_{\scriptscriptstyle\mathrm{B}}$ are the Fermi and Bose distributions, respectively. This is a limit of the results in ref. [36]. At high temperatures the potential can be approximated as

$$\mathcal{V}(m) \;\overset{m\ll\pi T}{\approx}\; -\frac{1}{4\pi^2}\int_0^\infty \mathrm{d}q\, q\left[n_{\scriptscriptstyle\mathrm{F}}(q)+n_{\scriptscriptstyle\mathrm{B}}(q)\right] = -\frac{T^2}{16}\;, \tag{5.11}$$

which directly leads to eq. (5.6) [37]. At low temperatures we get

$$\mathcal{V}(m) \;\overset{m\gg\pi T}{\approx}\; \frac{4k^2}{3\pi^2 m^4}\int_0^\infty \mathrm{d}q\, q^3\, n_{\scriptscriptstyle\mathrm{F}}(q) = \frac{7\pi^2T^4k^2}{90m^4}\;, \tag{5.12}$$

which corresponds to the result in ref. [38] (cf. also refs. [39, 40]).

For a numerical evaluation, the q-integral in eq. (5.10) can be divided into two ranges as $\int_0^\infty \mathrm{d}q = \int_0^{q_*}\mathrm{d}q + \int_{q_*}^\infty \mathrm{d}q$ and the ϵ-integral as $\int_m^\infty \mathrm{d}\epsilon = \int_m^{\epsilon_*}\mathrm{d}\epsilon + \int_{\epsilon_*}^\infty \mathrm{d}\epsilon$, where

$$q_* \;\equiv\; \frac{m^2}{4k}\;, \quad \epsilon_* \;\equiv\; \sqrt{m^2+\left(\frac{m^2-4k^2}{4k}\right)^2}\;. \tag{5.13}$$

Then numerical evaluation poses no problems; the result is illustrated in figure 5.

5.3 Interaction rate from $1+n \leftrightarrow 2+n$ scatterings

We now move on to Γ as defined by eq. (5.8), frequently called the active neutrino width or damping or interaction rate. The $1+n \leftrightarrow 2+n$ contributions to Γ are illustrated in figure 1(b), and correspond physically to the decays $W^\pm, Z^0, \gamma \to \ell N$. From the kinematics point of view these processes are similar to those appearing in the direct contribution of section 3.2, if we simply replace the Goldstone modes by gauge fields; the difference is that the cubic coupling is now g rather than h. Thus, in the Feynman R_ξ gauge in which gauge field propagators are similar to scalar propagators and no additional structures appear,[8] the parametric magnitude of these processes is $\delta k_0\Gamma \sim g^2m^2 \sim g^4T^2$. This turns out to be of NNLO compared with the contribution from $2\to 2$ scatterings, and is therefore negligible at high temperatures.

[8] In other gauges the longitudinal combination $Q_\mu Q_\nu/m_{\scriptscriptstyle W}^2$ appears in the gauge field propagator. This leads to large $\mathcal{O}(\pi^2/g^2)$ effects for $q\sim\pi T, m_{\scriptscriptstyle W}\sim gT$ and violates our power counting setup.

JCAP07(2016)015

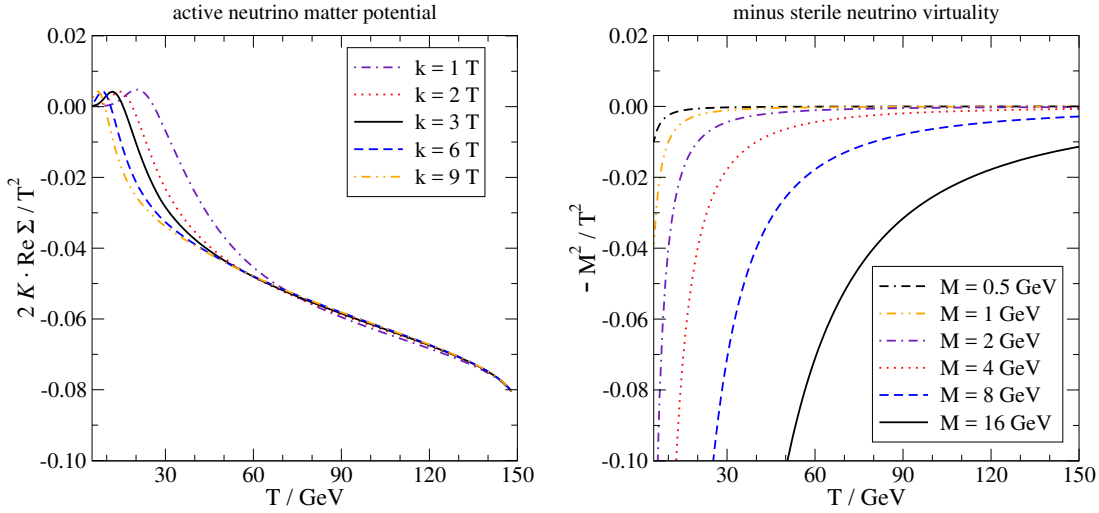

Figure 5. Quantities characterizing the active neutrino propagator, eq. (5.4). Left: the real part of the active neutrino self-energy, or "finite-temperature matter potential", $2\mathcal{K}\cdot\mathrm{Re}\,\Sigma/T^2$, from eq. (5.9). The high-temperature limit is given by eq. (5.6), and the low-temperature limit corresponds to the Fermi model, cf. eq. (5.12). Right: minus the sterile neutrino mass squared in the same units. The crossing of the two curves implies a "resonant" conversion from active to sterile neutrinos, however the resonance is parametrically fairly broad because of a large width $k_0\Gamma$, cf. eq. (2.13) and figure 6.

At low temperatures, when $m_W \gtrsim k_0 \sim \pi T$, there is no need for resummation, cf. section 3.3.[9] Then the relevant $1 \leftrightarrow 2$ processes are the decays of the $W^\pm$ and Z^0 gauge bosons. We can write a Born rate like in eq. (3.31),

$$k_0\,\Gamma^{\rm Born} \;=\; (g_1^2+g_2^2)\,\mathcal{F}(m_Z) + 2g_2^2\,\mathcal{F}(m_W)\;, \tag{5.14}$$

where $\mathcal{F}$ is from eq. (3.32). It is appropriate to remark that Γ is gauge independent only on the mass-shell of active neutrinos, i.e. $M \to 0$, in accordance with eq. (5.8). Thereby we obtain

$$\mathcal{F}(m) \;\stackrel{M\to 0}{\longrightarrow}\; \frac{m^2 T}{32\pi k}\ln\biggl\{\frac{1+e^{-\frac{m^2}{4kT}}}{1-e^{-\frac{1}{T}(k+\frac{m^2}{4k})}}\biggr\}\;. \tag{5.15}$$

The contribution of eq. (5.14) in this limit is illustrated in figure 6 ("Born $1\leftrightarrow 2$"), and it represents the dominant process for $T \lesssim 30\,\mathrm{GeV}$.

5.4 Interaction rate from $2 \leftrightarrow 2$ scatterings with hard momentum transfer

We now turn to the $2 \to 2$ contribution to Γ. Proceeding first with Feynman diagrams, the result can be written in a form analogous to the direct contribution in eq. (4.1):

$$\begin{aligned} 2n_{\rm F}(k_0)\;k_0\Gamma\big|^{\rm hard}_{2\,\to\,2} \;=\; \int \mathrm{d}\Omega_{2\to 2}\,\biggl\{ & n_{\rm B}(p_1)\,n_{\rm B}(p_2)\,\bigl[1-n_{\rm F}(k_1)\bigr]\,\frac{1}{2}\sum|\mathcal{M}_{\rm d}|^2 \\ & + n_{\rm B}(p_1)\,n_{\rm F}(p_2)\,\bigl[1+n_{\rm B}(k_1)\bigr]\,\sum|\mathcal{M}_{\rm e}|^2 \\ & + n_{\rm F}(p_1)\,n_{\rm F}(p_2)\,\bigl[1-n_{\rm F}(k_1)\bigr]\,\sum|\mathcal{M}_{\rm f}|^2\biggr\}\;. \end{aligned} \tag{5.16}$$

[9] Resummation becomes important when the ultrarelativistic $1\leftrightarrow 2$ and the full $1+n\leftrightarrow 2+n$ LPM lines depart from each other in figure 3, i.e. $T \gtrsim 60\,\mathrm{GeV}$.

JCAP07(2016)015

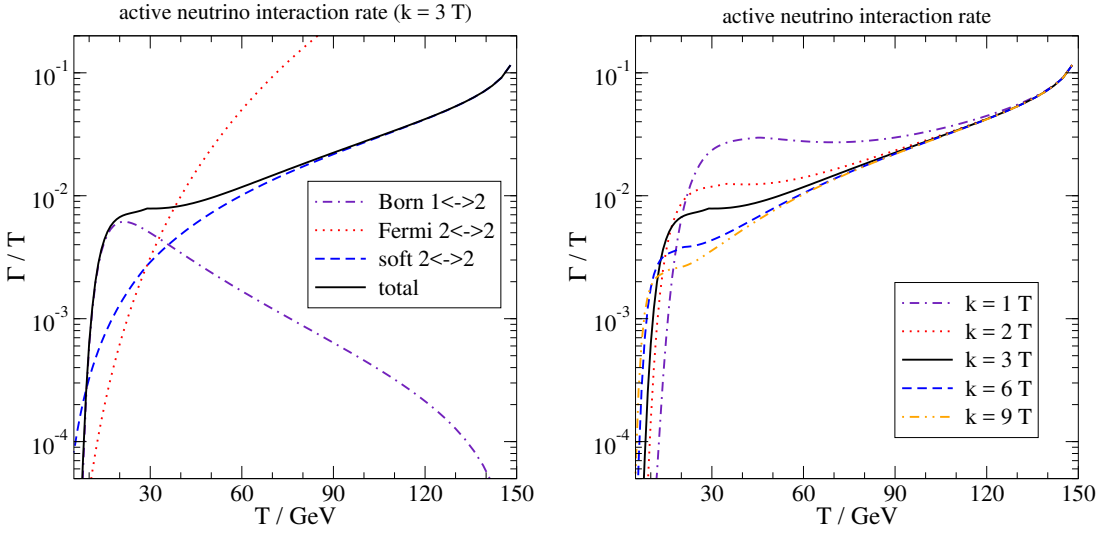

Figure 6. The active neutrino interaction rate, defined in eq. (5.8). Shown are the Born rate from eq. (5.14) ("Born 1 ↔ 2"), the Fermi model result for 2 ↔ 2 scatterings from eq. (5.34) ("Fermi 2 ↔ 2"), and the soft 2 ↔ 2 scattering contribution from eq. (5.33) ("soft 2 ↔ 2"). The total result has been obtained by taking the smaller between the Fermi and the soft 2 ↔ 2 scattering results, which limits both to their ranges of applicability, and adding to it the Born 1 ↔ 2 rate. On the right, the total rate is shown for a number of momenta.

The corresponding diagrams are shown in figure 7. In the massless limit (this will be rectified below), we obtain

$$\sum |\mathcal{M}_{\rm d}|^2 \equiv -\left(6g_2^4 + \frac{g_1^4+3g_2^4}{2}n_S\right)\left(\frac{u^2+t^2}{s^2}\right) + \frac{n_S}{2}(g_1^4+3g_2^4) + \left(\frac{g_1^2+3g_2^2}{2}\right)^2\left(\frac{u}{t}+\frac{t}{u}\right), \tag{5.17}$$

$$\sum |\mathcal{M}_{\rm e}|^2 \equiv \left(6g_2^4 + \frac{g_1^4+3g_2^4}{2}n_S\right)\left(\frac{u^2+s^2}{t^2}\right) - \frac{n_S}{2}(g_1^4+3g_2^4) - \left(\frac{g_1^2+3g_2^2}{2}\right)^2\left(\frac{u}{s}+\frac{s}{u}\right), \tag{5.18}$$

$$\sum |\mathcal{M}_{\rm f}|^2 \equiv \left(3g_2^4+\frac{5}{3}g_1^4\right)n_G\left(\frac{u^2+s^2}{t^2}+\frac{u^2+t^2}{s^2}+\frac{t^2+s^2}{u^2}\right) + \frac{3}{4}(g_1^4+6g_1^2g_2^2-3g_2^4)\,. \tag{5.19}$$

In order to simplify the last equation we have symmetrized the integrand in $p_1 \leftrightarrow p_2$ and made use of the identity $u^2/(st)+t^2/(su)+s^2/(ut)=3$. If the phase space integrals were finite (which they are not), eqs. (5.17)–(5.19) would suggest that $k_0\Gamma \sim g^4T^2$.

In analogy with eq. (4.10), the phase space can be reduced into a 2-dimensional one:

$$k_0\Gamma\big|^{\rm hard}_{2\to 2} = \frac{1}{(4\pi)^3 k_0}\int_{k_0}^{\infty}{\rm d}q_+\int_0^{k_0}{\rm d}q_-\Big\{\big[n_{\rm B}(q_0)+n_{\rm F}(q_0-k_0)\big]\,\Xi_{s1} + \big[n_{\rm F}(q_0)+n_{\rm B}(q_0-k_0)\big]\,\Xi_{s2}\Big\}$$

JCAP07(2016)015

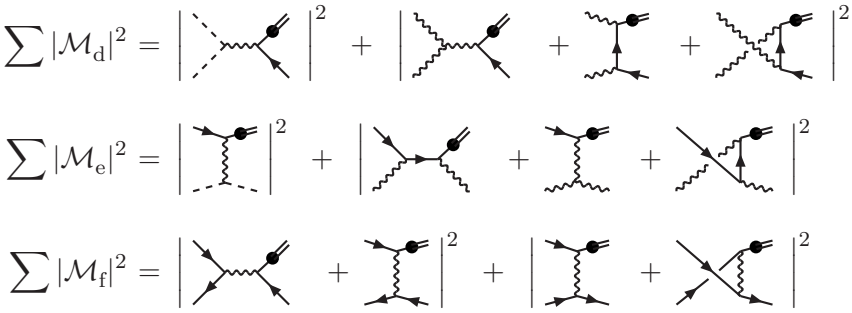

Figure 7. $2 \to 2$ scattering processes contributing to eqs. (5.17)–(5.19). The notation is like in figure 1.

$$+\frac{1}{(4\pi)^3 k_0}\int_0^{k_0}\mathrm{d}q_+\int_{-\infty}^{0}\mathrm{d}q_-\Big\{\big[1+n_{\rm B}(q_0)-n_{\rm F}(k_0-q_0)\big]\,\Xi_{t1} + \big[1-n_{\rm F}(q_0)+n_{\rm B}(k_0-q_0)\big]\,\Xi_{t2}\Big\}\,. \quad (5.20)$$

The most important case Ξ_{t1} corresponds to bosonic t-channel exchange. The functions appearing in eq. (5.20) are given in appendix C.

The s-channel functions Ξ_{s1} and Ξ_{s2} remain finite in the whole integration range. In contrast, the t-channel functions Ξ_{t1} and Ξ_{t2} have non-integrable divergences at $q, q_0 \ll k_0$:

$$\begin{aligned}\Xi_{t1} \,=\, & \left(6g_2^4+\frac{g_1^4+3g_2^4}{2}n_S\right)\left\{\frac{\pi^2T^2q_0}{3q^4}\Big[3(q_0-2k_0)^2-q^2\Big]\right. \\ & \left.+\frac{k_0(q_0-k_0)T}{q^4}\left[6q_0q+(q^2-3q_0^2)\ln\frac{q+q_0}{q-q_0}\right]+\frac{k_0^2q_0(q^2-q_0^2)}{2q^4}\right\} \\ & +\left(6g_2^4+\frac{10}{3}g_1^4\right)n_G\left\{\frac{\pi^2T^2q_0}{6q^4}\Big[3(q_0-2k_0)^2-q^2\Big]-\frac{k_0^2q_0(q^2-q_0^2)}{2q^4}\right\}+\mathcal{O}(1)\,, \quad (5.21)\end{aligned}$$

$$\Xi_{t2} \,=\, \left(\frac{g_1^2+3g_2^2}{2}\right)^2\frac{k_0\pi^2T^2}{q^2}+\mathcal{O}\left(\frac{1}{q}\right)\,. \quad (5.22)$$

Here all terms that need to be subtracted in order for the integrals to be finite have been shown; in eq. (5.21) one more order is needed, because the multiplier of Ξ_{t1} in eq. (5.20) contains the divergent factor $n_{\rm B}(q_0)$.

It may be noted that eq. (5.22) has precisely the same type of logarithmic divergence as eq. (4.14). In contrast, eq. (5.21) leads to a power-divergent integral. This indicates that our naive estimate concerning the magnitude of $k_0\Gamma$ is incorrect; in fact soft gauge scatterings boost the width, so that its correct magnitude is $k_0\Gamma \sim g^4T^4/(g^2T^2) \sim g^2T^2$. We now turn to the determination of this IR contribution.

5.5 Interaction rate from $2 \leftrightarrow 2$ scatterings with soft momentum transfer

The particle mediating soft t-channel exchange in figure 7 can be either a gauge boson or a lepton. However only one particle can be soft at a time. We start by briefly discussing the simpler case that the exchanged particle is a lepton, because the analysis is then analogous to that in eqs. (4.15)-(4.22), however in the end this contribution will turn out to be parametrically subdominant (it amounts to an NNLO contribution).

JCAP07(2016)015

When the lepton is soft, the gauge boson is hard. A hard gauge boson can be treated like a free massless particle in the symmetric phase. Then the HTL contribution looks much like in eqs. (4.15) and (4.17),

$$k_0\Gamma|_{2\to 2}^{\text{HTL-lepton}} = \frac{g_1^2+3g_2^2}{4}\int_{-\infty}^{\infty}\mathrm{d}q_0\int_{\mathbf{q}}\frac{-2\mathcal{K}\cdot\rho_\ell(q_0,\mathbf{q})}{|\mathbf{k}-\mathbf{q}|} \times\big[1-n_{\mathrm{F}}(q_0)+n_{\mathrm{B}}(k_0-q_0)\big]\,\delta(k_0-q_0-|\mathbf{k}-\mathbf{q}|) \tag{5.23}$$

$$\approx \frac{g_1^2+3g_2^2}{8\pi^2}\int_{-\infty}^{k_0}\mathrm{d}q_0\int_{|q_0|}^{2k_0-q_0}\mathrm{d}q\,q\,q_0\,(\hat\rho_s-\hat\rho_0)(q_0,q)\left[n_{\mathrm{B}}(k_0)+\frac{1}{2}\right]. \tag{5.24}$$

We again treat this in two different ways. A subtraction term is obtained by expanding like in eq. (4.18), and yields

$$k_0\Gamma|_{2\to 2}^{\text{HTL-lepton, expanded}} = \frac{g_1^2+3g_2^2}{32\pi}\int_{-\infty}^{k_0}\mathrm{d}q_0\int_{|q_0|}^{2k_0-q_0}\mathrm{d}q\,\frac{m_\ell^2}{q^2}\left[n_{\mathrm{B}}(k_0)+\frac{1}{2}\right]. \tag{5.25}$$

This agrees with the divergence originating from eq. (5.22). The philosophy is to subtract eq. (5.25) from eq. (5.20), and add the corresponding "soft" contribution from eq. (5.24) in its proper form. Following eq. (4.22), we readily obtain

$$k_0\Gamma|_{2\to 2}^{\text{HTL-lepton, soft}} \approx \frac{(g_1^2+3g_2^2)m_\ell^2}{16\pi}\ln\!\left(\frac{2k_0}{m_\ell}\right)\left[n_{\mathrm{B}}(k_0)+\frac{1}{2}\right], \tag{5.26}$$

where terms of $\mathcal{O}(m_\ell/k_0)$ were omitted. With eq. (5.25) subtracted and eq. (5.26) added, the indirect contribution from the function Ξ_{t2} to $k_0\Gamma|_{2\to 2}$ is finite and of $\mathcal{O}(g^4T^2)$.

If, in contrast, the lepton is hard, it can be treated like a free massless particle in the symmetric phase. The exchanged gauge boson needs now to be HTL resummed. We get[10]

$$\begin{aligned} k_0\Gamma|_{2\to 2}^{\text{HTL-gauge}} &= \int_{-\infty}^{\infty}\mathrm{d}q_0\int_{\mathbf{q}}\frac{\big[1+n_{\mathrm{B}}(q_0)-n_{\mathrm{F}}(k_0-q_0)\big]\,\delta(k_0-q_0-|\mathbf{k}-\mathbf{q}|)}{2|\mathbf{k}-\mathbf{q}|} \\ &\quad\times\left\{2g_2^2\left[\frac{k_0^2q_\perp^2(\rho_{\mathrm{T}2}-\rho_{\mathrm{E}2})(q_0,q)}{q^2}+\frac{(q^2-q_0^2)\rho_{\mathrm{T}2}(q_0,q)}{2}\right]+(g_1^2+g_2^2)\big[2\to Z\big]\right\} \\ &= \frac{1}{8\pi^2k_0}\int_{-\infty}^{k_0}\mathrm{d}q_0\int_{|q_0|}^{2k_0-q_0}\mathrm{d}q\,q\,\big[1+n_{\mathrm{B}}(q_0)-n_{\mathrm{F}}(k_0-q_0)\big] \\ &\quad\times\left\{2g_2^2\left[\frac{k_0^2q_\perp^2(\rho_{\mathrm{T}2}-\rho_{\mathrm{E}2})(q_0,q)}{q^2}+\frac{(q^2-q_0^2)\rho_{\mathrm{T}2}(q_0,q)}{2}\right]+(g_1^2+g_2^2)\big[2\to Z\big]\right\}, \end{aligned} \tag{5.27}$$

where (for $k=k_0$)

$$q_\perp^2 \;\equiv\; q^2-q_\parallel^2 \;\equiv\; q^2-\frac{(\mathbf{k}\cdot\mathbf{q})^2}{k^2} \;=\; \frac{(q^2-q_0^2)[(q_0-2k_0)^2-q^2]}{4k_0^2}. \tag{5.28}$$

The HTL spectral functions $\rho_{\mathrm{T}2}$, $\rho_{\mathrm{E}2}$, $\rho_{\mathrm{T}Z}$, $\rho_{\mathrm{E}Z}$ are given in appendix B.

[10] Vertex corrections are of higher order and can be omitted.

JCAP07(2016)015

We again treat the soft contribution in eq. (5.27) in two different ways. A subtraction term is obtained by going to the symmetric phase, like in the computation based on eqs. (5.17)–(5.19), and expanding like in eq. (4.18). For $q, q_0 \gg gT$ this yields

$$\frac{k_0^2 q_\perp^2 (\rho_{\mathrm{T}i} - \rho_{\mathrm{E}i})(q_0, q)}{q^2} + \frac{(q^2 - q_0^2)\rho_{\mathrm{T}i}(q_0, q)}{2} \approx \frac{\pi m_{\mathrm{E}i}^2 q_0}{16 q^5} \left[3(q_0 - 2k_0)^2 - q^2\right] , \quad i \in \{1, 2\} . \tag{5.29}$$

Thereby

$$k_0 \Gamma|_{2\to 2}^{\text{HTL-gauge, expanded}} = \frac{g_1^2 m_{\mathrm{E}1}^2 + 3 g_2^2 m_{\mathrm{E}2}^2}{128\pi k_0} \times \int_{-\infty}^{k_0} \mathrm{d}q_0 \int_{|q_0|}^{2k_0 - q_0} \mathrm{d}q \left[1 + n_{\mathrm{B}}(q_0) - n_{\mathrm{F}}(k_0 - q_0)\right] \frac{q_0}{q^4} \left[3(q_0 - 2k_0)^2 - q^2\right] . \tag{5.30}$$

Inserting the masses from eq. (3.4) this agrees exactly with the leading $1/q^4$ divergence as shown in eq. (5.21).

The philosophy is thus to subtract eq. (5.30) from eq. (5.20), and add the corresponding "soft" contribution from eq. (5.27) in its proper form. The soft contribution originates from $q, q_0 \sim m_{\mathrm{E}i} \ll k_0$. Changing variables from q to $q_\perp$ (cf. eq. (5.28)) the leading contribution from eq. (5.27) (in an expansion in $\mathcal{O}(m_{\mathrm{E}i}^2/k_0^2)$) becomes

$$k_0 \Gamma|_{2\to 2}^{\text{HTL-gauge, soft}} \approx \frac{k_0 T}{8\pi^2} \int_{-\infty}^{k_0} \mathrm{d}q_0 \int_0^{2k_0} \mathrm{d}q_\perp \, q_\perp \frac{2 g_2^2 (\rho_{\mathrm{T}2} - \rho_{\mathrm{E}2}) + (g_1^2 + g_2^2)(\rho_{\mathrm{T}Z} - \rho_{\mathrm{E}Z})}{q_0} \frac{q_\perp^2}{q_\perp^2 + q_0^2} . \tag{5.31}$$

At this point we can change the order of integrations like in eq. (4.22) and make use of a sum rule derived in refs. [31, 32],

$$\int_{-\infty}^{\infty} \frac{\mathrm{d}q_0}{\pi} \frac{\rho_{\mathrm{T}2} - \rho_{\mathrm{E}2}}{q_0} \left(q_0, \sqrt{q_0^2 + q_\perp^2}\right) \frac{q_\perp^2}{q_\perp^2 + q_0^2} = \frac{1}{q_\perp^2 + m_W^2} - \frac{1}{q_\perp^2 + m_{\widetilde{W}}^2} . \tag{5.32}$$

This structure corresponds to that in the Matsubara zero-mode sector, and equals the integrand in eq. (3.17). Similarly, the Z channel case leads to the integrand in eq. (3.18). The integral over $q_\perp$ can now be carried out, yielding

$$k_0 \Gamma|_{2\to 2}^{\text{HTL}-\text{gauge, soft}} = \frac{k_0 T}{8\pi} \left\{ 2 g_2^2 \ln \frac{m_{\widetilde{W}}}{m_W} + (g_1^2 + g_2^2) \left[\cos^2(\theta - \tilde{\theta}) \ln \frac{m_{\widetilde{Z}}}{m_Z} + \sin^2(\theta - \tilde{\theta}) \ln \frac{m_{\widetilde{Q}}}{m_Z} \right] \right\} + \mathcal{O}\left(\frac{g^2 T m_{\mathrm{E}2}^2}{k_0}\right) . \tag{5.33}$$

We note that eq. (5.33) is of $\mathcal{O}(g^2 T^2)$ and is finite in the broken phase. In the notation of eq. (3.20), $\Gamma|_{2\to 2}^{\text{HTL}-\text{gauge, soft}} = 2\Gamma_{\,W}(0) + \Gamma_{\,Z}(0)$. Eq. (5.33) is among our main results.

Given that eq. (5.33) represents an IR sensitive result, being dominated by momentum transfer of $\mathcal{O}(gT)$, it could experience large radiative corrections. In fact, as is typical of observables determined by the Debye scale, these are only suppressed by $\mathcal{O}(g/\pi)$. We have not computed these NLO corrections, but a way to do this is outlined in appendix D. Let us stress again that, in contrast, the contribution from hard momentum transfer is of $\mathcal{O}(g^4 T^2)$, i.e. NNLO, once the IR sensitive parts have been subtracted and treated properly.

The result of eq. (5.33) is illustrated numerically in figure 6 ("soft $2 \leftrightarrow 2$"). It dominates the active neutrino interaction rate at $T \gtrsim 40\,\mathrm{GeV}$.

JCAP07(2016)015

5.6 Limit of low temperatures

At low temperatures, $m_W \gtrsim gT$, the mass ratios appearing in eq. (5.33) behave as $m_{\widetilde{W}}^2/m_W^2 \approx 1 + m_{\rm E2}^2/m_W^2$, so that the interaction rate decreases as $k_0\Gamma \sim k_0\, g^4T^3/m_W^2$. This is not the correct low-temperature asymptotics, however; the approximations made break down when $m_W \gg gT$, and the correct form is $k_0\Gamma \sim k_0^2\, g^4T^4/m_W^4$. This asymptotics can be computed within the Fermi model. The corresponding results have been tabulated, up to $T \sim 10\,$GeV, on the web page related to ref. [19]. For completeness we specify here the result for $5\,{\rm GeV} \lesssim T \lesssim 30\,{\rm GeV}$ in a form which is easily amenable to a numerical evaluation.

Adding the contribution of the bottom quark to the processes listed in ref. [19]; going to the limit $M \to 0$ in which the result is gauge independent; and making use of the same variables as in eqs. (4.5)–(4.10), we obtain

$$\begin{aligned} k_0\Gamma|^{\rm Fermi}_{2\to 2} = {} & \frac{1}{(4\pi)^3 k_0}\int_{k_0}^{\infty}{\rm d}q_+\int_0^{k_0}{\rm d}q_-\,\Big[n_{\rm B}(q_0)+n_{\rm F}(q_0-k_0)\Big]\,\Xi_{s1} \\ & + \frac{1}{(4\pi)^3 k_0}\int_0^{k_0}{\rm d}q_+\int_{-\infty}^{0}{\rm d}q_-\,\Big[1+n_{\rm B}(q_0)-n_{\rm F}(k_0-q_0)\Big]\,\Xi_{t1}\,. \end{aligned} \tag{5.34}$$

The functions appearing read

$$\Xi_{s1} \,=\, 16\,A\,G_{\rm F}^2\,(q_0^2-q^2)^2\,\Big[q+2T(\ln_{\rm f}^{+}-\ln_{\rm f}^{-})\Big]\,, \tag{5.35}$$

$$\Xi_{t1} \,=\, 16\,A\,G_{\rm F}^2\,(q_0^2-q^2)^2\,\Big[2T(\ln_{\rm f}^{-}-\ln_{\rm f}^{+})\Big]\,, \tag{5.36}$$

where $G_{\rm F}$ is the Fermi constant, and

$$A \equiv \frac{15}{2} - 2s^2 + 12s^4 + N_{\rm c}\left[\frac{5}{2} - \frac{14s^2}{3} + \frac{44s^4}{9} + 2\Big(|V_{\rm ud}|^2 + |V_{\rm us}|^2 + |V_{\rm cd}|^2 + |V_{\rm cs}|^2\Big)\right]\,. \tag{5.37}$$

Here $s = \sin\theta$ is the weak mixing angle, defined like below eq. (3.9), and $|V_{\rm ub}|^2$ and $|V_{\rm cb}|^2$ have been omitted as vanishingly small. Numerically, the integral evaluates to $k_0\Gamma \approx 10 G_{\rm F}^2 T^4 k_0^2$. The result is illustrated in figure 6 ("Fermi $2 \leftrightarrow 2$").

6 Numerical results

The contributions of sections 3 (direct $1{+}n \leftrightarrow 2{+}n$ scatterings), 4 (direct $2 \leftrightarrow 2$ scatterings), and 5 (indirect contributions), are collected together into figure 8. It is immediately clear that the indirect contribution dominates at low temperatures by several orders of magnitude. However, the smaller M is, the sooner does the direct contribution take over, because the indirect rate is proportional to M^2, cf. eq. (2.12).

The total rate, obtained by summing together the direct and indirect contributions from figure 8, is shown in figure 9. The k-dependence is illustrated in more detail for $M = 0.5\,$GeV and $M = 2.0\,$GeV in figure 10.[11] Various physical quantities can be obtained by weighting these rates appropriately and integrating over the spectrum (cf. eqs. (2.6), (2.7) and (2.9)). Because of the appearance of the Fermi distribution in these weights, the phase space is dominated by $k \sim 3T$. Two examples of physically relevant quantities are discussed in the next section.

[11] Tabulated results for full spectra can be downloaded from www.laine.itp.unibe.ch/production-midT/. This web site also lists the active neutrino interaction rate shown in figure 6(right) and the lepton number washout rate shown in figure 11(right).

JCAP07(2016)015

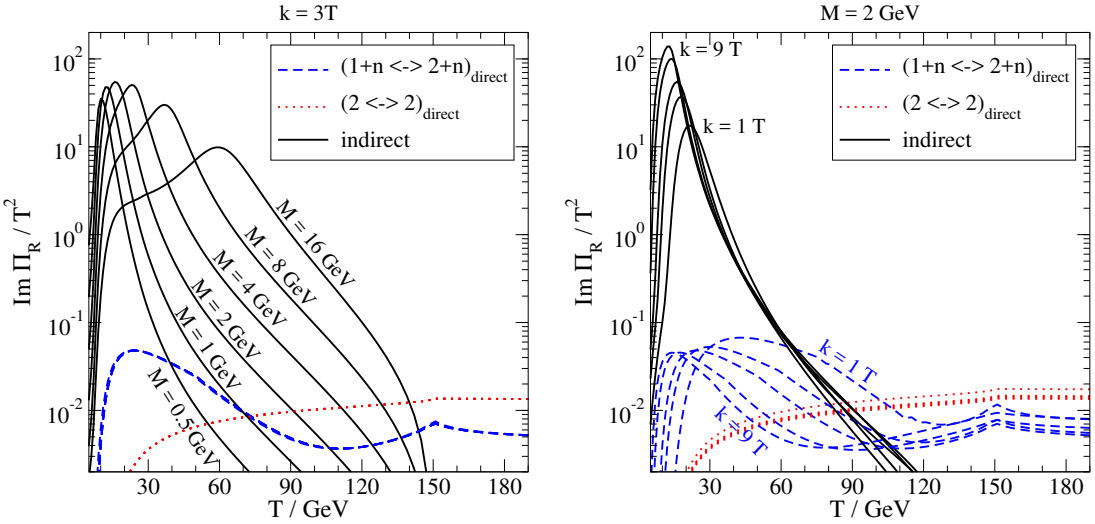

Figure 8. Various contributions to $\mathrm{Im}\,\Pi_{\mathrm{R}}/T^2$. Shown are the direct $1+n \leftrightarrow 2+n$ scatterings from section 3 (dashed lines); the direct $2 \leftrightarrow 2$ scatterings from section 4 (dotted lines); as well as the full indirect contribution from section 5 (solid lines). Left: fixed $k = 3T$ and masses $M/\mathrm{GeV} \in \{0.5, \ldots, 16\}$. Right: fixed $M = 2\,\mathrm{GeV}$ and momenta $k/T \in \{1, 2, 3, 6, 9\}$.

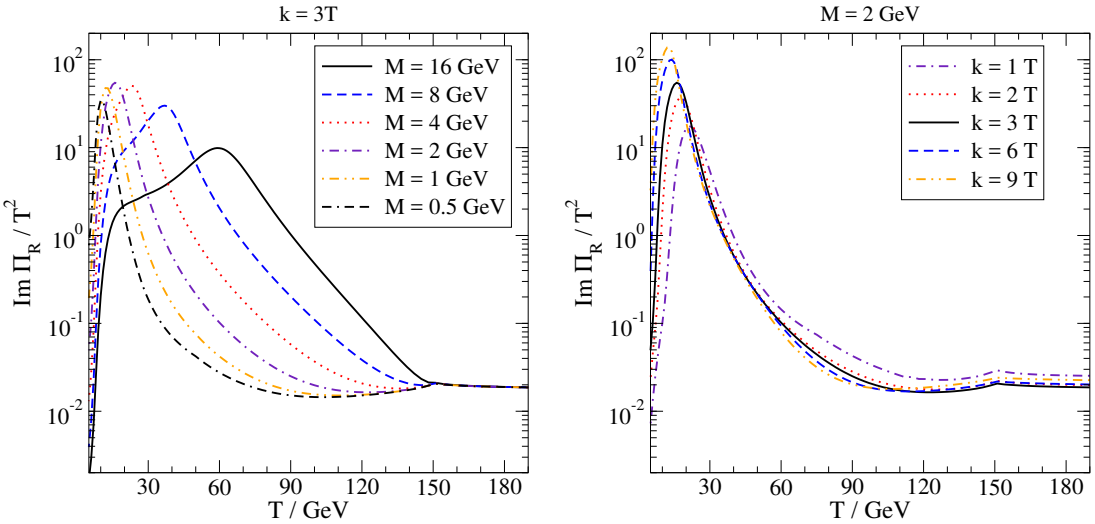

Figure 9. The full $\mathrm{Im}\,\Pi_{\mathrm{R}}/T^2$, obtained by summing together the contributions from figure 8. Left: fixed $k = 3T$. Right: fixed $M = 2\,\mathrm{GeV}$. Corresponding results for $T < 10\,\mathrm{GeV}$ and $T > 160\,\mathrm{GeV}$ have been tabulated in ref. [29].

7 Conclusions

For $T < 160\,\mathrm{GeV}$ so that the Higgs mechanism is operative, the equilibration rate of a right-handed neutrino of mass M (cf. eq. (2.6)) can be split into "direct" and "indirect" contributions (cf. eq. (2.11)). These correspond to different types of scatterings as illustrated in figures 1 and 2. In the ultrarelativistic regime, where all particle masses are $\ll \pi T$, the indirect contribution can in turn be expressed in terms of the left-handed neutrino "asymptotic thermal mass", m_ℓ, and "interaction rate", Γ, as indicated by eq. (2.12). At lower temperatures the general structure remains intact even though m_ℓ gets replaced by a more complicated (momentum-dependent) function, as has been reviewed in section 5.2.

JCAP07(2016)015

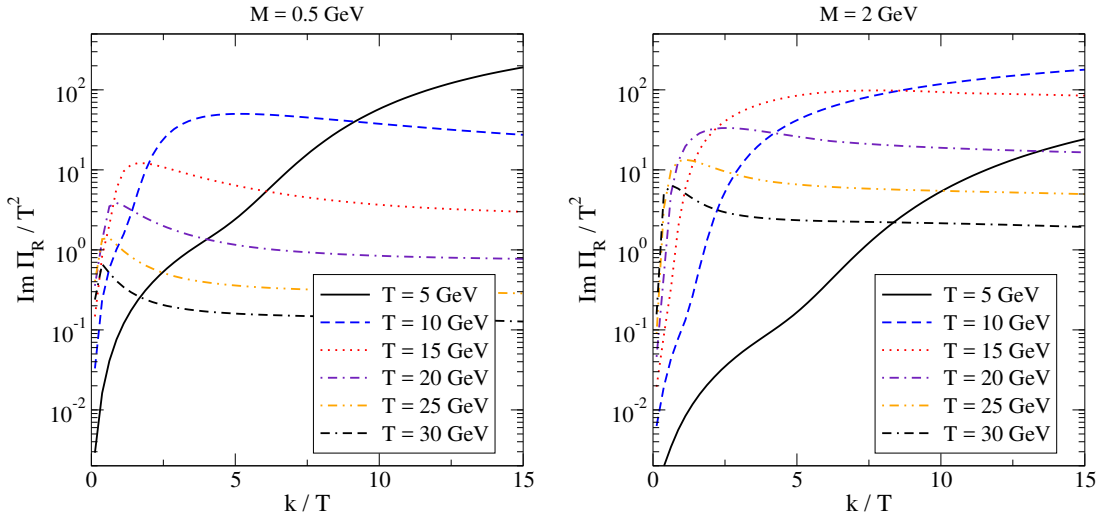

Figure 10. The dependence of $\mathrm{Im}\,\Pi_{\mathrm{R}}/T^2$ on k for $M = 0.5\,\mathrm{GeV}$ (left) and $M = 2\,\mathrm{GeV}$ (right). The spectra at these and other temperatures can be downloaded as explained in footnote 11.

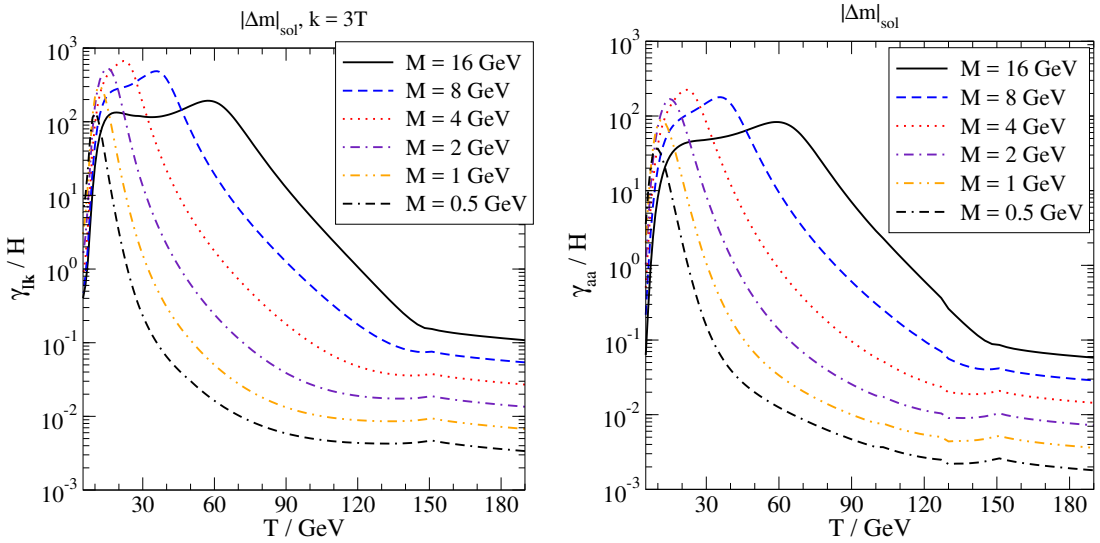

Figure 11. Left: the right-handed neutrino equilibration rate compared with the Hubble rate, cf. eq. (7.1), for $k = 3T$. Active neutrino masses correspond to $|\Delta m|_{\mathrm{sol}} \approx 8.7 \times 10^{-3}\,\mathrm{eV}$; for the atmospheric neutrino value $|\Delta m|_{\mathrm{atm}} \approx 4.9 \times 10^{-2}\,\mathrm{eV}$ the rate is faster by a factor ~ 5.6. Right: the (diagonal) lepton number washout rate compared with the Hubble rate, cf. eq. (2.8).

We have shown that in the regime $T \gtrsim 40\,\mathrm{GeV}$, the active neutrino interaction rate Γ is dominated by t-channel scatterings mediated by soft gauge boson exchange (referred to as the "soft $2 \leftrightarrow 2$" contribution in figure 6). In this situation Γ is "large", $\Gamma \sim g^2 T/\pi$. The explicit expression is fairly simple, cf. eq. (5.33). This large contribution originates from contributions sensitive to momenta $\sim gT$ which would be quadratically infrared divergent without the appropriate HTL resummation. There is also a subleading (linear) infrared divergence in eq. (5.21) whose origin can also be understood (cf. appendix D).

For the masses $M \sim 0.5 \ldots 2.0\,\mathrm{GeV}$, relevant for the SHiP experiment [14], the right-handed neutrino equilibration rate peaks at low temperatures, $T \sim 5 \ldots 30\,\mathrm{GeV}$ (cf. figure 9).

JCAP07(2016)015

In this regime the active neutrino interaction rate Γ is dominated by $1 \to 2$ decays (cf. figure 6) and $\mathrm{Im}\,\Pi_{\mathrm{R}}$ is dominated by the indirect contribution (cf. figure 8). It is again possible to express the dominant contribution to Γ in a simple analytic form, cf. eqs. (5.14) and (5.15).

In order to illustrate the physics significance of these results, let us first compare the right-handed neutrino equilibration rate $\gamma_{I\mathbf{k}}$ from eq. (2.6) with the Hubble rate $H = \sqrt{8\pi e/(3m_{\mathrm{Pl}}^2)}$, where e is the energy density of the universe and m_{Pl} is the Planck mass. For simplicity we consider a seesaw scenario with hierarchical neutrinos, and assume that only one neutrino Yukawa coupling contributes to a given mass difference. Then active neutrino mass differences are of the form $|\Delta m| = |h_{Ia}|^2 v^2/(2M)$, whereby we can eliminate $|h_{Ia}|^2$ from $\gamma_{I\mathbf{k}}$ to get

$$\frac{\gamma_{I\mathbf{k}}}{H} \;=\; 1.39 \times 10^5 \times \left|\frac{\Delta m}{\mathrm{eV}}\right| \times \frac{M}{k_0} \times \frac{\mathrm{Im}\,\Pi_{\mathrm{R}}}{\sqrt{e(T)}}\,. \tag{7.1}$$

Inserting e as tabulated in ref. [41] (cf. also ref. [42]), the result is illustrated in figure 11(left). We conclude that in the mass range $M \sim 0.5 \ldots 16\,\mathrm{GeV}$ right-handed neutrinos do equilibrate at temperatures above $T = 5\,\mathrm{GeV}$. Increasing the mass above 4 GeV decreases the peak equilibration rate but broadens the temperature range in which the rate is substantial.

Turning to our main observable, the lepton number washout rate from eq. (2.8), the flavour-diagonal part of the result is shown in figure 11(right). The flavour non-diagonal rate is an order of magnitude slower because of the smaller inverse susceptibility, cf. figure 12(right). The flavour-diagonal rate exceeds the Hubble rate for all masses considered. However we note that this equilibration dynamics rapidly switches off in the range $T \lesssim 4\,\mathrm{GeV}$ in which dark matter computations have been carried out [19–21].

The results of figure 11(right) indicate that leptogenesis based on right-handed neutrinos with few GeV masses remains an interesting possibility, because these degrees of freedom do not equilibrate at $T \gtrsim 130\,\mathrm{GeV}$ when sphaleron processes are active [43]. In contrast it is difficult to generate a large lepton asymmetry for low temperatures, which could boost dark matter production in the scenario of ref. [3], because at $T \lesssim 30\,\mathrm{GeV}$ lepton number violating reactions are in equilibrium and therefore an efficient washout process takes place. It should be acknowledged, however, that we have not performed a detailed phenomenological scan of the whole parameter space, so the existence of fine-tuned regions where the window may remain open cannot be excluded. The numerical results tabulated as explained in footnote 11 should hopefully permit for further work to be carried out in this direction.

Acknowledgments

M.L. thanks D. Bödeker and M. Shaposhnikov for valuable discussions. The work was supported by the Swiss National Science Foundation (SNF) under grant 200020-155935, and by the Väisälä Foundation.

A Lepton number susceptibility matrix

Here we compute the susceptibility matrix defined below eq. (2.9) to leading order in Standard Model couplings. Two regimes are considered: $5\,\mathrm{GeV} \lesssim T \lesssim 130\,\mathrm{GeV}$ so that $B+L$ violation is out of thermal equilibrium [43]; and $T \gtrsim 130\,\mathrm{GeV}$ so that $B+L$ violation is in equilibrium. The methods of the computation have been discussed in refs. [18, 20], whereas the general approach dates back to ref. [44].

JCAP07(2016)015

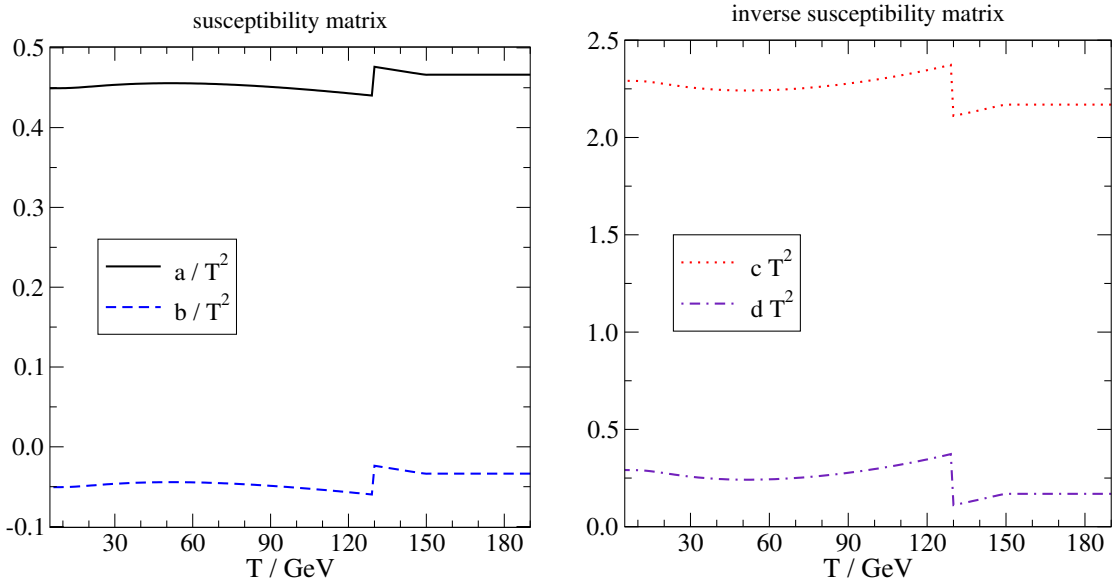

Figure 12. The coefficients a and b determining the lepton number susceptibility matrix (cf. eq. (A.1)) and c and d determining its inverse (cf. eq. (A.2)). The apparent discontinuity at $T = 130\,\mathrm{GeV}$ originates from the fact that the $B+L$ violating rate was assumed to be in equilibrium at $T > 130\,\mathrm{GeV}$ and out of equilibrium at $T < 130\,\mathrm{GeV}$. Treating this regime precisely requires solving a non-equilibrium problem with a finite $B + L$ violating rate [43], however in practice it may be sufficient to solve separate non-equilibrium problems on both sides and connect the solutions continuously.

Given that at $T \gtrsim 5\,\mathrm{GeV}$ all lepton flavours are degenerate, the susceptibility matrix $\Xi_{ab} = \partial n_a/\partial\mu_b$ takes the form

$$\Xi = \begin{pmatrix} a & b & b \\ b & a & b \\ b & b & a \end{pmatrix} . \tag{A.1}$$

Its inverse, playing a role in eq. (2.9), reads

$$\Xi^{-1} = \begin{pmatrix} c & d & d \\ d & c & d \\ d & d & c \end{pmatrix} , \quad c = \frac{a+b}{(a-b)(a+2b)} , \quad d = \frac{-b}{(a-b)(a+2b)} . \tag{A.2}$$

The functions $a, \ldots, d$ are plotted in figure 12. We now give details concerning the computation.

The computation proceeds by assigning chemical potentials μ_a to the different lepton densities; the chemical potential μ_q to the quark number density; and by denoting the zero components of the gauge potentials by

$$\mu_{_Y} \equiv ig_1 B_0 , \quad \mu_{_A} \equiv ig_2 A_0^3 . \tag{A.3}$$

In the regime $T > 130\,\mathrm{GeV}$, the quark chemical potential is eliminated through the sphaleron constraint $\mu_q = -\frac{1}{9}\sum_a \mu_a$, whereas for $T < 130\,\mathrm{GeV}$ it is expressed in terms of a baryon chemical potential as $\mu_q = \mu_{_B}/3$; subsequently we make a Legendre transform to an ensemble with a fixed baryon density $n_{_B}$ and then set $n_{_B} \to 0$ in comparison with lepton densities. The gauge potentials $\mu_{_Y}$ and $\mu_{_A}$ are eliminated by requiring charge neutrality, $\partial p/\partial\mu_{_Y} =$

$\partial p/\partial\mu_{_A} = 0$, where $p = -\Omega/V$ is the pressure, Ω is the grand canonical potential, and V is the volume. Subsequently, $\Xi_{ab} = \frac{\partial^2 p}{\partial\mu_a\partial\mu_b}$.

The contributions of various particle species to p are parametrized by the susceptibilities

$$\chi_{\rm F}(m) \equiv \int_{\mathbf{p}}\big[-2n'_{\rm F}(E)\big] \;=\; \frac{m^2}{\pi^2}\sum_{n=1}^{\infty}(-1)^{n+1}K_2\biggl(\frac{nm}{T}\biggr) \;\stackrel{m\to 0}{\to}\; \frac{T^2}{6}\;, \tag{A.4}$$

$$\chi_{\rm B}(m) \equiv \int_{\mathbf{p}}\big[-2n'_{\rm B}(E)\big] \;=\; \frac{m^2}{\pi^2}\sum_{n=1}^{\infty}K_2\biggl(\frac{nm}{T}\biggr) \;\stackrel{m\to 0}{\to}\; \frac{T^2}{3}\;, \tag{A.5}$$

where K_2 is a modified Bessel function. At leading order[12] we obtain

$$\begin{aligned} p(T,\mu) - p(T,0) \,=\, & \chi_{\rm F}(0)\biggl[12\mu_q^2 + 4\mu_{_Y}\mu_q + \sum_a\frac{3\mu_a^2}{2} - 2\mu_{_Y}\sum_a\mu_a + \frac{9\mu_{_A}^2}{4} + \frac{49\mu_{_Y}^2}{12}\biggr] \\ & + \chi_{\rm F}(m_t)\biggl[3\mu_q^2 - \frac{3\mu_{_A}\mu_q}{2} + \frac{5\mu_{_Y}\mu_q}{2} + \frac{3\mu_{_A}^2}{8} - \frac{\mu_{_A}\mu_{_Y}}{4} + \frac{17\mu_{_Y}^2}{24}\biggr] \\ & + \chi_{\rm F}(m_b)\biggl[3\mu_q^2 + \frac{3\mu_{_A}\mu_q}{2} - \frac{\mu_{_Y}\mu_q}{2} + \frac{3\mu_{_A}^2}{8} + \frac{\mu_{_A}\mu_{_Y}}{4} + \frac{5\mu_{_Y}^2}{24}\biggr] \\ & + \Bigl[\chi_{\rm B}(m_\phi) + \chi_{\rm B}(m_{_Z})\Bigr]\frac{(\mu_{_A}+\mu_{_Y})^2}{16} \;+\; \chi_{\rm B}(m_{_W})\biggl[\frac{9\mu_{_A}^2}{8} - \frac{\mu_{_A}\mu_{_Y}}{4} + \frac{\mu_{_Y}^2}{8}\biggr] \\ & + \frac{v^2(\mu_{_A}+\mu_{_Y})^2}{8} \;+\; \mathcal{O}\biggl(\frac{gv\mu^2 T}{4\pi}, \frac{g^2v^2\mu^2}{16\pi^2}, \mu^4\biggr)\;, \end{aligned} \tag{A.6}$$

where $v^2 \simeq -m_\phi^2/\lambda$ is the thermal Higgs expectation value and μ denotes generically all chemical potentials. It can be checked that for $\mu_q, \mu_a \to 0$ and taking the temperature to be larger than all masses, this expression reproduces the Debye masses in eq. (3.4).

As far as the coefficients in eqs. (A.1) and (A.2) are concerned, for the regime $T > 130\,\mathrm{GeV}$ a straightforward minimization leads to

$$c - d = \frac{1}{a-b} = \frac{1}{3\chi_{\rm F}(0)}\;. \tag{A.7}$$

The other linear combinations have more complicated expressions, for instance

$$\frac{a}{2} = \chi_{11} + \frac{\chi_{1Y}^2\chi_{AA} - \chi_{1A}\chi_{1Y}\chi_{AY} + \chi_{1A}^2\chi_{YY}}{\chi_{AY}^2 - 4\chi_{AA}\chi_{YY}}\;, \tag{A.8}$$

where the χ's are combinations of susceptibilities coupling to different chemical potentials:

$$\chi_{11} \;=\; \frac{89\chi_{\rm F}(0)}{54} + \frac{\chi_{\rm F}(m_t)+\chi_{\rm F}(m_b)}{27}\;, \tag{A.9}$$

$$\chi_{1A} \;=\; \frac{\chi_{\rm F}(m_t)-\chi_{\rm F}(m_b)}{6}\;, \tag{A.10}$$

$$\chi_{1Y} \;=\; -\frac{22\chi_{\rm F}(0)}{9} + \frac{\chi_{\rm F}(m_b)-5\chi_{\rm F}(m_t)}{18}\;, \tag{A.11}$$

[12] We stress that the gauge boson contribution is treated consistently only in the regimes $m_{_W} \ll \pi T$ and $m_{_W} \gg \pi T$. For $m_{_W} \sim gT$ the mass dependence amounts to a correction of $\mathcal{O}(g)$ which is not correctly represented by this expression. For $m_{_W} \sim \pi T$ the susceptibilities are parametrically of the same order as the unknown $\mathcal{O}(g^2)$ corrections and do not constitute any theoretically well-defined subset thereof.

JCAP07(2016)015

$$\chi_{AA} = \frac{v^2}{8} + \frac{9\chi_{\rm F}(0)}{4} + \frac{3[\chi_{\rm F}(m_t)+\chi_{\rm F}(m_b)]}{8} + \frac{\chi_{\rm B}(m_\phi)+\chi_{\rm B}(m_Z)+18\chi_{\rm B}(m_W)}{16}\,, \tag{A.12}$$

$$\chi_{AY} = \frac{v^2}{4} + \frac{\chi_{\rm F}(m_b)-\chi_{\rm F}(m_t)}{4} + \frac{\chi_{\rm B}(m_\phi)+\chi_{\rm B}(m_Z)-2\chi_{\rm B}(m_W)}{8}\,, \tag{A.13}$$

$$\chi_{YY} = \frac{v^2}{8} + \frac{49\chi_{\rm F}(0)}{12} + \frac{17\chi_{\rm F}(m_t)+5\chi_{\rm F}(m_b)}{24} + \frac{\chi_{\rm B}(m_\phi)+\chi_{\rm B}(m_Z)+2\chi_{\rm B}(m_W)}{16}\,. \tag{A.14}$$

Going to the symmetric phase, it can be checked that the resulting expressions for c and d agree with the leading-order results given in ref. [18].

For the regime $T < 130\,\mathrm{GeV}$, we may first eliminate μ_q from the requirement of vanishing baryon density, whereby eqs. (A.9)–(A.14) get replaced with

$$\chi_{11} = \frac{3\chi_{\rm F}(0)}{2}\,, \quad \chi_{1A} = 0\,, \quad \chi_{1Y} = -2\chi_{\rm F}(0)\,, \tag{A.15}$$

$$\chi_{AA} = \frac{v^2}{8} + \frac{15\chi_{\rm F}(0)}{4} + \frac{\chi_{\rm B}(m_\phi)+\chi_{\rm B}(m_Z)+18\chi_{\rm B}(m_W)}{16} + \frac{3[\chi_{\rm F}^2(m_t)+6\chi_{\rm F}(m_t)\chi_{\rm F}(m_b)+\chi_{\rm F}^2(m_b)-32\chi_{\rm F}^2(0)]}{16[4\chi_{\rm F}(0)+\chi_{\rm F}(m_t)+\chi_{\rm F}(m_b)]}\,, \tag{A.16}$$

$$\chi_{AY} = \frac{v^2}{4} + \frac{\chi_{\rm B}(m_\phi)+\chi_{\rm B}(m_Z)-2\chi_{\rm B}(m_W)}{8} + \frac{3[\chi_{\rm F}(m_t)-\chi_{\rm F}(m_b)]^2}{8[4\chi_{\rm F}(0)+\chi_{\rm F}(m_t)+\chi_{\rm F}(m_b)]}\,, \tag{A.17}$$

$$\chi_{YY} = \frac{v^2}{8} + \frac{21\chi_{\rm F}(0)}{4} + \frac{\chi_{\rm B}(m_\phi)+\chi_{\rm B}(m_Z)+2\chi_{\rm B}(m_W)}{16} + \frac{3[\chi_{\rm F}^2(m_t)+6\chi_{\rm F}(m_t)\chi_{\rm F}(m_b)+\chi_{\rm F}^2(m_b)-32\chi_{\rm F}^2(0)]}{16[4\chi_{\rm F}(0)+\chi_{\rm F}(m_t)+\chi_{\rm F}(m_b)]}\,. \tag{A.18}$$

Eq. (A.7) and the form of eq. (A.8) remain unchanged. At low temperatures the expressions agree with those given in ref. [20]. Numerical results are shown in figure 12.

The numerical uncertainties of the leading-order susceptibilities have been discussed in refs. [18, 30]. Because of effects of the QCD gauge coupling on quark number susceptibilities, and because of infrared sensitive bosonic effects only suppressed by $\mathcal{O}(g)$, uncertainties are expected to be on the $\sim 20\%$ level.

B Hard Thermal Loop resummed leptons and gauge bosons

For completeness we list in this appendix the Hard Thermal Loop resummed [34, 35] spectral functions corresponding to the lepton and gauge field propagators in the regime where the masses of these particles, including the contribution from the Higgs mechanism, are parametrically at most of $\mathcal{O}(gT)$.

The lepton spectral function, defined as a four-vector originating from the imaginary part of the retarded propagator, has the form

$$\rho_\ell(q_0,\mathbf{q}) \equiv \Big(q_0\,\hat{\rho}_0(q_0,q), \mathbf{q}\,\hat{\rho}_s(q_0,q)\Big)\,, \tag{B.1}$$

$$\hat{\rho}_0(q_0,q) = \mathrm{Im}\left\{\frac{1-\frac{m_\ell^2 L}{2q_0}}{\left[q_0-\frac{m_\ell^2 L}{2}\right]^2-\left[q+\frac{m_\ell^2(1-q_0 L)}{2q}\right]^2}\right\}\,, \tag{B.2}$$

$$\hat{\rho}_s(q_0,q) = \mathrm{Im}\left\{\frac{1+\frac{m_\ell^2(1-q_0 L)}{2q^2}}{\left[q_0-\frac{m_\ell^2 L}{2}\right]^2-\left[q+\frac{m_\ell^2(1-q_0 L)}{2q}\right]^2}\right\}\,, \tag{B.3}$$

JCAP07(2016)015

where $L \equiv \frac{1}{2q} \ln \frac{q_0+q}{q_0-q}$ and q_0 has a small positive imaginary part, so that $\mathrm{Im}\, L = -\pi/(2q)$ for $q > q_0$. The "asymptotic" thermal mass appearing in these equations is given in eq. (3.2).

The gauge field spectral function also contains two independent structures, associated with the (imaginary-time) projectors

$$\mathbb{P}^{\mathrm{T}}_{\mu\nu}(Q) \equiv \delta_{\mu i}\delta_{\nu j}\left(\delta_{ij} - \frac{q_i q_j}{q^2}\right), \tag{B.4}$$

$$\mathbb{P}^{\mathrm{E}}_{\mu\nu}(Q) \equiv \delta_{\mu\nu} - \frac{Q_\mu Q_\nu}{Q^2} - \mathbb{P}^{\mathrm{T}}_{\mu\nu}(Q)\,. \tag{B.5}$$

For $W^\pm$ the spectral functions corresponding to these projections read

$$\rho_{\mathrm{T}2}(q_0,q) = \mathrm{Im}\left\{\frac{1}{q^2 - q_0^2 + m_W^2 + \Pi_{\mathrm{T}2}}\right\}, \quad \Pi_{\mathrm{T}2} \equiv \frac{m_{\mathrm{E}2}^2}{2q^2}\Big[q_0^2 + q_0(q^2-q_0^2)L\Big], \tag{B.6}$$

$$\rho_{\mathrm{E}2}(q_0,q) = \mathrm{Im}\left\{\frac{1}{q^2 - q_0^2 + m_W^2 + \Pi_{\mathrm{E}2}}\right\}, \quad \Pi_{\mathrm{E}2} \equiv \frac{m_{\mathrm{E}2}^2(q^2-q_0^2)}{q^2}\Big[1 - q_0\, L\Big], \tag{B.7}$$

where again q_0 has a small positive imaginary part, and $m_{\mathrm{E}2}^2$ is from eq. (3.4). The Z-channel spectral function, appearing in eqs. (5.27) and (5.31), is more complicated because the self-energies lead to a different mixing angle than in vacuum. It can be expressed as

$$\rho_{\mathrm{T}Z} \equiv \mathrm{Im}\left\{\frac{q^2 - q_0^2 + c^2\Pi_{\mathrm{T}1} + s^2\Pi_{\mathrm{T}2}}{(q^2-q_0^2)^2 + (q^2-q_0^2)(m_Z^2 + \Pi_{\mathrm{T}1} + \Pi_{\mathrm{T}2}) + m_Z^2(c^2\Pi_{\mathrm{T}1} + s^2\Pi_{\mathrm{T}2}) + \Pi_{\mathrm{T}1}\,\Pi_{\mathrm{T}2}}\right\}, \tag{B.8}$$

and correspondingly for $\rho_{\mathrm{E}Z}$, where the weak mixing angles c, s have been defined around eq. (3.9). The self-energy $\Pi_{\mathrm{T}1}$ is like $\Pi_{\mathrm{T}2}$ in eq. (B.6) but with the replacement $m_{\mathrm{E}2} \to m_{\mathrm{E}1}$. In the symmetric phase, i.e. $m_Z \to 0$, the Z channel spectral function simplifies into

$$\rho_{\mathrm{T}Z} = s^2\rho_{\mathrm{T}1} + c^2\rho_{\mathrm{T}2}\,, \tag{B.9}$$

so that $(g_1^2+g_2^2)\rho_{\mathrm{T}Z} = \sum_{i=1}^2 g_i^2\rho_{\mathrm{T}i}$. Finally, we note that the photon and the mixed photon-Z propagators can be expressed in a form similar to eq. (B.8),

$$\rho_{\mathrm{T}Q} \equiv \mathrm{Im}\left\{\frac{q^2 - q_0^2 + m_Z^2 + s^2\Pi_{\mathrm{T}1} + c^2\Pi_{\mathrm{T}2}}{\Delta}\right\}, \tag{B.10}$$

$$\rho_{\mathrm{T}ZQ} \equiv \mathrm{Im}\left\{\frac{cs(\Pi_{\mathrm{T}1} - \Pi_{\mathrm{T}2})}{\Delta}\right\}, \tag{B.11}$$

where Δ is the denominator of eq. (B.8).

C Integrated matrix elements for indirect $2 \leftrightarrow 2$ processes

We list in this appendix the functions defined in eq. (5.20), obtained after carrying out all but two of the phase space integrals in eq. (5.16). Making use of the notation of eqs. (4.5)–(4.9) we get

$$\begin{aligned}\Xi_{s1} = {} & \frac{n_S}{4}\big(g_1^4 + 3g_2^4\big)\left[q + 2T(\ln_{\mathrm{b}}^+ - \ln_{\mathrm{b}}^-)\right] \\ & + \frac{3}{4}\big(g_1^4 + 6g_1^2g_2^2 - 3g_2^4\big)\left[q + 2T(\ln_{\mathrm{f}}^+ - \ln_{\mathrm{f}}^-)\right]\end{aligned}$$

$$
\begin{aligned}
&-\left(6g_2^4+\frac{g_1^4+3g_2^4}{2}n_S\right)\left\{\frac{q}{3}+\frac{T}{2q^2}\big[q^2+(q_0-2k_0)^2\big](\ln_{\rm b}^+-\ln_{\rm b}^-)\right.\\
&\left.+\frac{T^2}{q^3}\big[q^2-3(q_0-2k_0)^2\big]\left[\mathrm{li}_{2\rm b}^+ + \mathrm{li}_{2\rm b}^- + \frac{2T}{q}\big(\mathrm{li}_{3\rm b}^+ - \mathrm{li}_{3\rm b}^-\big)\right]\right\}\\
&+\left(6g_2^4+\frac{10}{3}g_1^4\right)n_G\left\{\frac{q}{3}+\frac{T}{2q^2}\big[q^2+(q_0-2k_0)^2\big](\ln_{\rm f}^+-\ln_{\rm f}^-)\right.\\
&\left.+\frac{T^2}{q^3}\big[q^2-3(q_0-2k_0)^2\big]\left[\mathrm{li}_{2\rm f}^+ + \mathrm{li}_{2\rm f}^- + \frac{2T}{q}\big(\mathrm{li}_{3\rm f}^+ - \mathrm{li}_{3\rm f}^-\big)\right]\right\}, \qquad \text{(C.1)}
\end{aligned}
$$

$$
\begin{aligned}
\Xi_{s2} = &-\frac{n_S}{2}\big(g_1^4+3g_2^4\big)\left[q+T(\ln_{\rm b}^+ + \ln_{\rm f}^+ - \ln_{\rm b}^- - \ln_{\rm f}^-)\right]\\
&+\left(\frac{g_1^2+3g_2^2}{2}\right)^2\left\{\frac{q}{2}+\frac{T}{q}\big[(k_0-q_-)(\ln_{\rm f}^+-\ln_{\rm b}^-)+(k_0-q_+)(\ln_{\rm f}^- - \ln_{\rm b}^+)\big]\right.\\
&\left.+\frac{T^2}{q^2}(2k_0-q_0)\big(\mathrm{li}_{2\rm b}^+ + \mathrm{li}_{2\rm f}^- - \mathrm{li}_{2\rm f}^+ - \mathrm{li}_{2\rm b}^-\big)\right\}, \qquad \text{(C.2)}
\end{aligned}
$$

$$
\begin{aligned}
\Xi_{t1} = &\left(6g_2^4+\frac{g_1^4+3g_2^4}{2}n_S\right)\left\{\frac{T}{2q^2}\big[q^2+(q_0-2k_0)^2\big](\ln_{\rm b}^+-\ln_{\rm b}^-)\right.\\
&\left.+\frac{T^2}{q^3}\big[q^2-3(q_0-2k_0)^2\big]\left[\mathrm{li}_{2\rm b}^+ - \mathrm{li}_{2\rm b}^- + \frac{2T}{q}\big(\mathrm{li}_{3\rm b}^+ - \mathrm{li}_{3\rm b}^-\big)\right]\right\}\\
&-\left(6g_2^4+\frac{10}{3}g_1^4\right)n_G\left\{\frac{T}{2q^2}\big[q^2+(q_0-2k_0)^2\big](\ln_{\rm f}^+-\ln_{\rm f}^-)\right.\\
&\left.+\frac{T^2}{q^3}\big[q^2-3(q_0-2k_0)^2\big]\left[\mathrm{li}_{2\rm f}^+ - \mathrm{li}_{2\rm f}^- + \frac{2T}{q}\big(\mathrm{li}_{3\rm f}^+ - \mathrm{li}_{3\rm f}^-\big)\right]\right\}, \qquad \text{(C.3)}
\end{aligned}
$$

$$
\begin{aligned}
\Xi_{t2} = &\left(\frac{g_1^2+3g_2^2}{2}\right)^2\left\{\frac{T}{q}\big[(k_0-q_-)(\ln_{\rm f}^+-\ln_{\rm b}^-)+(k_0-q_+)(\ln_{\rm f}^- - \ln_{\rm b}^+)\big]\right.\\
&\left.+\frac{T^2}{q^2}(2k_0-q_0)\big(\mathrm{li}_{2\rm b}^+ + \mathrm{li}_{2\rm b}^- - \mathrm{li}_{2\rm f}^+ - \mathrm{li}_{2\rm f}^-\big)\right\}. \qquad \text{(C.4)}
\end{aligned}
$$

D Towards soft momentum transfer at next-to-leading order

In section 5.5 we accounted for the leading divergence at $q, q_0 \ll k_0$ given in eq. (5.21). Let us now show that the origin of the next-to-leading divergence can be understood as well.

If we change variables from q to $q_\perp$, defined in eq. (5.28), and integrate over q_0, then Γ can be expressed as an integral over $q_\perp$. It turns out that the integrand is equivalent to the "transverse collision kernel", $C(q_\perp)$, determined up to NLO in QCD in the domain $q_\perp \sim m_{\rm E}$ in ref. [32], or the elastic scattering cross section, $\mathrm{d}\Gamma_{\rm el}/\mathrm{d}^2\mathbf{q}_\perp$, determined up to $\mathcal{O}(g^4)$ for $q_\perp \gg m_{\rm E}$ in ref. [45]. Concretely, eq. (20) of ref. [32] can for $q_\perp \gg m_{\rm E}$ be expanded as

$$
C(q_\perp) \overset{q_\perp \gg m_{\rm E}}{=} g^2 T C_{\rm F}\left[\frac{m_{\rm E}^2}{q_\perp^4} - \frac{g^2 T C_{\rm A}}{16 q_\perp^3} + \mathcal{O}\big(g^4T^2\big)\right], \qquad \text{(D.1)}
$$

where $C_{\rm F} \equiv (N_{\rm c}^2-1)/(2N_{\rm c})$ and $C_{\rm A} \equiv N_{\rm c}$ are Casimir factors related to the fundamental and adjoint representation, respectively. We now show that the NLO divergence in eq. (5.21) amounts precisely to the NLO term in eq. (D.1).

Let us introduce a scale Λ in the range $gT \ll \Lambda \ll k_0$ and consider the contribution to eq. (5.20) from momenta $q \leq \Lambda$. In this domain $q_\perp$ can be approximated as in eq. (4.21),

JCAP07(2016)015

and we can change variables according to

$$\int_0^\Lambda \mathrm{d}q \int_{-q}^{q} \mathrm{d}q_0\, f(q_0,q) = \int_0^\Lambda \mathrm{d}q_\perp\, q_\perp \int_{-\sqrt{\Lambda^2-q_\perp^2}}^{\sqrt{\Lambda^2-q_\perp^2}} \mathrm{d}q_0\, \frac{f\bigl(q_0,\sqrt{q_\perp^2+q_0^2}\bigr)}{\sqrt{q_\perp^2+q_0^2}}$$
$$= \int_0^\Lambda \mathrm{d}q_\perp\, q_\perp \int_1^{\Lambda/q_\perp} \mathrm{d}x \sum_{\sigma=\pm} \frac{f(\sigma\, q_\perp\sqrt{x^2-1}, q_\perp x)}{\sqrt{x^2-1}}\,. \tag{D.2}$$

The leading and NLO divergences originate from a domain where we can approximate

$$1 + n_{\mathrm{B}}(q_0) - n_{\mathrm{F}}(k_0-q_0) \approx \frac{T}{q_0}\,. \tag{D.3}$$

Thereby we are left with the integrals

$$\int_1^{\Lambda/q_\perp} \mathrm{d}x\, \frac{1}{x^4\sqrt{x^2-1}} = \frac{2}{3} + \mathcal{O}\biggl(\frac{q_\perp}{\Lambda}\biggr)\,, \tag{D.4}$$

$$\int_1^{\Lambda/q_\perp} \mathrm{d}x \biggl[\frac{6}{x^3\sqrt{x^2-1}} + \frac{3-2x^2}{x^4(x^2-1)} \ln\frac{x+\sqrt{x^2-1}}{x-\sqrt{x^2-1}}\biggr] = \frac{\pi^2}{2} + \mathcal{O}\biggl(\frac{q_\perp}{\Lambda}\biggr)\,. \tag{D.5}$$

Inserting these, the leading and NLO infrared divergences to Γ become

$$\Gamma_{2\to 2}^{\text{hard,expanded}} = \int_0^\Lambda \frac{\mathrm{d}^2\mathbf{q}_\perp}{(2\pi)^2} \biggl\{ \frac{g_1^2 T}{4}\biggl[\frac{m_{\mathrm{E1}}^2}{q_\perp^4} - \frac{g_1^2 T(\frac{n_S}{2})}{16 q_\perp^3}\biggr] + \frac{3g_2^2 T}{4}\biggl[\frac{m_{\mathrm{E2}}^2}{q_\perp^4} - \frac{g_2^2 T(2+\frac{n_S}{2})}{16 q_\perp^3}\biggr]\biggr\}\,. \tag{D.6}$$

The non-Abelian part agrees exactly with eq. (D.1) after inserting $C_{\mathrm{F}} = 3/4$ and $C_{\mathrm{A}} = 2$; the contribution from the Higgs field has a similar structure but a different group theory factor.

We conclude that accounting properly for the subleading divergence in eq. (5.21) would require an NLO computation similar to that performed in ref. [32] but generalized to the broken phase and including the contribution of the Higgs field.

E Fixing the parameters

Given that the computation presented in the main body of this paper is a leading-order one, without NLO logarithms to cancel the renormalization scale dependence, the choices that we make for the running parameters have some numerical significance. Our general approach follows that in ref. [29]. The running $\overline{\mathrm{MS}}$ parameters are fixed in terms of physical quantities (pole masses, Fermi constant) at a scale $\bar{\mu}_0 \equiv m_Z$, making use of the NLO relations specified in ref. [46]. The Higgs mass is set to $m_H = 125\,\mathrm{GeV}$. The renormalization scale appearing in the thermal computations is chosen as $\bar{\mu} \equiv \pi T$. If $\bar{\mu} > \bar{\mu}_0$, the couplings are evolved through 1-loop renormalization group equations. If $\bar{\mu} < \bar{\mu}_0$, whereby we find ourselves in a massive regime, the couplings are not evolved at all. We note that the strong gauge coupling, which should logically be evolved with 5 quark flavours in this regime, does not appear in our expressions at the current order. The Higgs expectation value is determined from the (resummed) leading-order expression $v^2 = -m_\phi^2/\lambda$, where m_ϕ^2 is the effective thermal Higgs mass parameter from eq. (3.2). With this procedure the electroweak "transition" takes in our results place at $T \approx 150\,\mathrm{GeV}$, whereas a non-perturbative investigation of the crossover region postpones it to $T \approx 160\,\mathrm{GeV}$ [42].

JCAP07(2016)015

References

[1] E.K. Akhmedov, V.A. Rubakov and A.Yu. Smirnov, *Baryogenesis via neutrino oscillations*, *Phys. Rev. Lett.* **81** (1998) 1359 [hep-ph/9803255] [INSPIRE].

[2] T. Asaka and M. Shaposhnikov, *The νMSM, dark matter and baryon asymmetry of the universe*, *Phys. Lett.* **B 620** (2005) 17 [hep-ph/0505013] [INSPIRE].

[3] X.-D. Shi and G.M. Fuller, *A new dark matter candidate: Nonthermal sterile neutrinos*, *Phys. Rev. Lett.* **82** (1999) 2832 [astro-ph/9810076] [INSPIRE].

[4] M. Shaposhnikov, *The νMSM, leptonic asymmetries and properties of singlet fermions*, *JHEP* **08** (2008) 008 [arXiv:0804.4542] [INSPIRE].

[5] T. Asaka, S. Eijima and H. Ishida, *Kinetic equations for baryogenesis via sterile neutrino oscillation*, *JCAP* **02** (2012) 021 [arXiv:1112.5565] [INSPIRE].

[6] B. Shuve and I. Yavin, *Baryogenesis through neutrino oscillations: a unified perspective*, *Phys. Rev.* **D 89** (2014) 075014 [arXiv:1401.2459] [INSPIRE].

[7] A. Abada, G. Arcadi, V. Domcke and M. Lucente, *Lepton number violation as a key to low-scale leptogenesis*, *JCAP* **11** (2015) 041 [arXiv:1507.06215] [INSPIRE].

[8] T. Hambye and D. Teresi, *Higgs doublet decay as the origin of the baryon asymmetry*, arXiv:1606.00017 [INSPIRE].

[9] M. Drewes, B. Garbrecht, D. Gueter and J. Klaric, *Leptogenesis from oscillations of heavy neutrinos with large mixing angles*, arXiv:1606.06690 [INSPIRE].

[10] P. Hernández, M. Kekic, J. López-Pavón, J. Racker and J. Salvado, *Testable baryogenesis in seesaw models*, arXiv:1606.06719 [INSPIRE].

[11] M. Drewes and B. Garbrecht, *Leptogenesis from a GeV seesaw without mass degeneracy*, *JHEP* **03** (2013) 096 [arXiv:1206.5537] [INSPIRE].

[12] P. Hernández, M. Kekic, J. López-Pavón, J. Racker and N. Rius, *Leptogenesis in GeV scale seesaw models*, *JHEP* **10** (2015) 067 [arXiv:1508.03676] [INSPIRE].

[13] P. Hernández, M. Kekic and J. Lopez-Pavon, $N_{\rm eff}$ *in low-scale seesaw models versus the lightest neutrino mass*, *Phys. Rev.* **D 90** (2014) 065033 [arXiv:1406.2961] [INSPIRE].

[14] S. Alekhin et al., *A facility to search for hidden particles at the CERN SPS: the SHiP physics case*, arXiv:1504.04855 [INSPIRE].

[15] R. Barbieri, P. Creminelli, A. Strumia and N. Tetradis, *Baryogenesis through leptogenesis*, *Nucl. Phys.* **B 575** (2000) 61 [hep-ph/9911315] [INSPIRE].

[16] S. Davidson, E. Nardi and Y. Nir, *Leptogenesis*, *Phys. Rept.* **466** (2008) 105 [arXiv:0802.2962] [INSPIRE].

[17] D. Bödeker, M. Sangel and M. Wörmann, *Equilibration, particle production and self-energy*, *Phys. Rev.* **D 93** (2016) 045028 [arXiv:1510.06742] [INSPIRE].

[18] D. Bödeker and M. Laine, *Kubo relations and radiative corrections for lepton number washout*, *JCAP* **05** (2014) 041 [arXiv:1403.2755] [INSPIRE].

[19] T. Asaka, M. Laine and M. Shaposhnikov, *Lightest sterile neutrino abundance within the νMSM*, *JHEP* **01** (2007) 091 [*Erratum ibid.* **02** (2015) 028] [hep-ph/0612182] [INSPIRE] and a related web page http://www.laine.itp.unibe.ch/neutrino-rate/.

[20] J. Ghiglieri and M. Laine, *Improved determination of sterile neutrino dark matter spectrum*, *JHEP* **11** (2015) 171 [arXiv:1506.06752] [INSPIRE].

[21] T. Venumadhav, F.-Y. Cyr-Racine, K.N. Abazajian and C.M. Hirata, *Sterile neutrino dark matter: A tale of weak interactions in the strong coupling epoch*, arXiv:1507.06655 [INSPIRE].

JCAP07(2016)015

[22] A. Salvio, P. Lodone and A. Strumia, *Towards leptogenesis at NLO: the right-handed neutrino interaction rate*, *JHEP* **08** (2011) 116 [arXiv:1106.2814] [INSPIRE].

[23] M. Laine and Y. Schröder, *Thermal right-handed neutrino production rate in the non-relativistic regime*, *JHEP* **02** (2012) 068 [arXiv:1112.1205] [INSPIRE].

[24] S. Biondini, N. Brambilla, M.A. Escobedo and A. Vairo, *An effective field theory for non-relativistic Majorana neutrinos*, *JHEP* **12** (2013) 028 [arXiv:1307.7680] [INSPIRE].

[25] B. Garbrecht, F. Glowna and M. Herranen, *Right-handed neutrino production at finite temperature: radiative corrections, soft and collinear divergences*, *JHEP* **04** (2013) 099 [arXiv:1302.0743] [INSPIRE].

[26] M. Laine, *Thermal right-handed neutrino production rate in the relativistic regime*, *JHEP* **08** (2013) 138 [arXiv:1307.4909] [INSPIRE].

[27] A. Anisimov, D. Besak and D. Bödeker, *Thermal production of relativistic Majorana neutrinos: Strong enhancement by multiple soft scattering*, *JCAP* **03** (2011) 042 [arXiv:1012.3784] [INSPIRE].

[28] D. Besak and D. Bödeker, *Thermal production of ultrarelativistic right-handed neutrinos: Complete leading-order results*, *JCAP* **03** (2012) 029 [arXiv:1202.1288] [INSPIRE].

[29] I. Ghisoiu and M. Laine, *Right-handed neutrino production rate at $T > 160\ GeV$*, *JCAP* **12** (2014) 032 [arXiv:1411.1765] [INSPIRE].

[30] D. Bödeker and M. Sangel, *Order g^2 susceptibilities in the symmetric phase of the Standard Model*, *JCAP* **04** (2015) 040 [arXiv:1501.03151] [INSPIRE].

[31] P. Aurenche, F. Gelis and H. Zaraket, *A simple sum rule for the thermal gluon spectral function and applications*, *JHEP* **05** (2002) 043 [hep-ph/0204146] [INSPIRE].

[32] S. Caron-Huot, *$O(g)$ plasma effects in jet quenching*, *Phys. Rev.* **D 79** (2009) 065039 [arXiv:0811.1603] [INSPIRE].

[33] M.J. Strassler and M.E. Peskin, *The heavy top quark threshold: QCD and the Higgs*, *Phys. Rev.* **D 43** (1991) 1500 [INSPIRE].

[34] J. Frenkel and J.C. Taylor, *Hard thermal QCD, forward scattering and effective actions*, *Nucl. Phys.* **B 374** (1992) 156 [INSPIRE].

[35] E. Braaten and R.D. Pisarski, *Simple effective Lagrangian for hard thermal loops*, *Phys. Rev.* **D 45** (1992) 1827 [INSPIRE].

[36] C. Quimbay and S. Vargas-Castrillón, *Fermionic dispersion relations in the standard model at finite temperature*, *Nucl. Phys.* **B 451** (1995) 265 [hep-ph/9504410] [INSPIRE].

[37] H.A. Weldon, *Effective fermion masses of order gT in high-temperature gauge theories with exact chiral invariance*, *Phys. Rev.* **D 26** (1982) 2789 [INSPIRE].

[38] D. Nötzold and G. Raffelt, *Neutrino dispersion at finite temperature and density*, *Nucl. Phys.* **B 307** (1988) 924 [INSPIRE].

[39] K. Enqvist, K. Kainulainen and J. Maalampi, *Refraction and oscillations of neutrinos in the early universe*, *Nucl. Phys.* **B 349** (1991) 754 [INSPIRE].

[40] J.C. D'Olivo, J.F. Nieves and M. Torres, *Finite temperature corrections to the effective potential of neutrinos in a medium*, *Phys. Rev.* **D 46** (1992) 1172 [INSPIRE].

[41] M. Laine and M. Meyer, *Standard Model thermodynamics across the electroweak crossover*, *JCAP* **07** (2015) 035 [arXiv:1503.04935] [INSPIRE].

[42] M. D'Onofrio and K. Rummukainen, *Standard model cross-over on the lattice*, *Phys. Rev.* **D 93** (2016) 025003 [arXiv:1508.07161] [INSPIRE].

JCAP07(2016)015

[43] M. D'Onofrio, K. Rummukainen and A. Tranberg, *Sphaleron rate in the Minimal Standard Model*, *Phys. Rev. Lett.* **113** (2014) 141602 [arXiv:1404.3565] [INSPIRE].

[44] S.Yu. Khlebnikov and M.E. Shaposhnikov, *Melting of the Higgs vacuum: conserved numbers at high temperature*, *Phys. Lett.* **B 387** (1996) 817 [hep-ph/9607386] [INSPIRE].

[45] P.B. Arnold and W. Xiao, *High-energy jet quenching in weakly-coupled quark-gluon plasmas*, *Phys. Rev.* **D 78** (2008) 125008 [arXiv:0810.1026] [INSPIRE].

[46] K. Kajantie, M. Laine, K. Rummukainen and M.E. Shaposhnikov, *Generic rules for high temperature dimensional reduction and their application to the Standard Model*, *Nucl. Phys.* **B 458** (1996) 90 [hep-ph/9508379] [INSPIRE].

JCAP07(2016)015